12:51:49 OCA PAD AMENDMENT - PROJECT HEADER INFORMATION 10/25/96

Active

Project #: B-15-F38 Cost share #: B-15-318 Rev #: 13
Center # : 10/24-6-R7674-0A0 Center shr #: 10/22-1-F7674-0A2 OCA file #:
Work type : RES
Contract#: 93-G-001 Mod #: ADMIN. Document : GRANT
Prime #: Contract entity: GTRC

Subprojects ? : N CFDA: 20.108
Main project #: PE #:

Project unit: ENGR COLL Unit code: 02.010.108
Project director(s):
ATLURI S N ENGR COLL (404)894-2758

Sponsor/division names: US DEPT OF TRANSPORTATION / FED AVIATION ADMIN
Sponsor/division codes: 124 / 008

Award period: 921020 to 960930 (performance) 960930 (reports)

Sponsor amount	New this change	Total to date
Contract value	0.00	2,250,000.00
Funded	0.00	2,250,000.00
Cost sharing amount		2,250,000.00

Does subcontracting plan apply ?: N

Title: CENTER OF EXCELLENCE IN COMPUTATIONAL MODELINGS OF AIRCRAFT STRUCTURES

PROJECT ADMINISTRATION DATA

OCA contact: Ina R. Lashley 894-4820

Sponsor technical contact	Sponsor issuing office
MICHAEL BASEHORE	PATRICIA WATTS
(609)485-6132	(609)485-5043
ENGINEERING, RESEARCH, & DEVELOPMENT SERVICE, ACD-1	OFFICE OF RESEARCH AND TECHNOLOGY APPLICATIONS
FAA TECHNICAL CENTER	FAA TECHNICAL CENTER
ALTANTIC CITY INTERNATIONAL AIRPORT, NJ 08405	ATLANTIC CITY INTERNATIONAL AIRPORT NJ 08405

Security class (U,C,S,TS) : U ONR resident rep. is ACO (Y/N): N
Defense priority rating : N/ supplemental sheet
Equipment title vests with: Sponsor GIT X

Administrative comments -
PROJECT # CHANGED IN OCA RECORDS FROM E-15-630 TO B-15-F38, IN COORDINATION
> WITH SANDY MASON (G&C ACCT0) AND PAUL SANDERS (CMC).

CA8120

Georgia Institute of Technology
Office of Contract Administration
PROJECT CLOSEOUT - NOTICE

Closeout Notice Date 29-DEC-1997

Project Number B-15-F38 Doch Id 35763

Center Number 10/24-6-R7674-0A0

Project Director ATLURI, SATYA

Project Unit ENGR COLL

Sponsor US DEPT OF TRANSPORTATION/FED AVIATION ADMIN

Division Id 3467

Contract Number 93-G-001 Contract Entity GTRC

Prime Contract Number

Title CENTER OF EXCELLENCE IN COMPUTATIONAL MODELINGS OF AIRCRAFT STRUCTURES

Effective Completion Date 30-SEP-1996 (Performance) 30-SEP-1996 (Reports)

Closeout Action:	Y/N	Date Submitted
Final Invoice or Copy of Final Invoice	Y	09-SEP-1997
Final Report of Inventions and/or Subcontracts	N	
Government Property Inventory and Related Certificate	N	
Classified Material Certificate	N	
Release and Assignment	N	
Other	N	

Comments

Distribution Required:

Project Director/Principal Investigator	Y
Research Administrative Network	Y
Accounting	Y
Research Security Department	N
Reports Coordinator	Y
Research Property Team	Y
Supply Services Department/Procurement	Y
Georgia Tech Research Corporation	Y
Project File	Y

B-15-F38
1

Thermal Gradients for Delamination Control

S. Hanagud
S.N. Atluri
L.N.B. Gummadi
C.C. McColl

School of Aerospace Engineering
FAA Center of Excellence for
Computational Modeling of Aircraft Structures
Georgia Institute of Technology
Atlanta, Georgia 30332

March 1994

Thermal Gradients for Delamination Control

S. Hanagud
S.N. Atluri
L.N.B. Gummadi
C.C. McColl

School of Aerospace Engineering
FAA Center of Excellence for
Computational Modeling of Aircraft Structures
Georgia Institute of Technology
Atlanta, Georgia 30332

March 1994

Contents

ABSTRACT

In this report, we have studied the feasibility of using thermal gradients to actively control the magnitude of interlaminar stresses. Interlaminar stresses are responsible for the development and growth of a delamination. Closed form analytical solutions have been obtained for interlaminar stresses in a laminated composite plate subjected to a combined mechanical and thermal loading. Thermal gradients required for reducing the magnitude of interlaminar stresses below a prescribed level are determined. Preliminary tests confirm the analytical results.

Chapter 1

INTRODUCTION

In the past, many passive techniques have been proposed to control interlaminar stresses and avoid the formation of delaminations. Pagano and Pipes [1] have suggested the use of a specific stacking order to eliminate the interlaminar tension. This technique can be used in the neighborhood of delamination-prone areas. However, a specific stacking sequence may defeat other design objectives. Pagano and Lackman [2] have shown that by serrating the fiber edges and filling in voids with the matrix material, the on-set of delamination can be prevented. Mignery et. al [3] have suggested sewing or wrapping the laminate in delamination prone areas. Chan et. al. [4] used a thin layer of tough adhesive at the interface of the fiber/matrix to delay the onset of delamination. In reference 5, Chan et. al studied the effect of parameters like the stacking sequence and the poisson's ratio on the interlaminar stresses. The focus of their studies was to prevent or delay the onset of a delamination. They did not consider techniques to arrest the growth of an existing delamination.

The only active control techniques to date, are proposed by Rogers et. al.[6] and Hanagud et. al. [7] and Gummadi[8]. In reference 6, authors have suggested a technique that incorporates strain induced actuators around the damage area. A proper actuation will reduce the stress concentration near the damage, thereby retarding

the damage growth. In references 7 and 8, the authors proposed an active control technique that involved detecting the delamination location and then controlling the growth of the detected delamination by using active control techniques.

1.1 PROBLEM SETTING

The objective of this report is to study the feasibility of using smart structure concepts to control delaminations in laminated composite structures. The growth of delaminations in a laminated composite structure can be arrested by reducing the interlaminar stresses that are responsible for the growth. An active control to reduce these interlaminar stresses needs actuators that can be used to counter the interlaminar stresses that are created by applied service loads. Several candidate actuators were considered. These include piezoelectric actuators, electrostrictive actuators, shape memory alloy actuators and imposed thermal gradients. In this report, we have restricted our studies to the use of imposed thermal gradients.

In order to explore the possible effectiveness of a thermal field in arresting the delaminations, we have selected a simple problem. In this simple problem, a layered composite plate of rectangular shape is considered. It is assumed that the plate is subjected to a uniform axial load along two parallel edges. In order to maintain the simplicity of the feasibility study, no pre-existing delaminations are considered. Instead, the feasibility study is focussed on the reduction of interlaminar stresses at the free edges of the rectangular plate.

In order to understand the structural mechanics of the actuation mechanism, analytical solutions are sought for the interlaminar stresses due to the applied axial forces and control forces transmitted by the actuators. In this study, imposed thermal fields transmit the needed control force.

Chapter 2

ANALYTICAL SOLUTIONS FOR INTERLAMINAR STRESSES

Nishioka and Atluri [9] used assumed equilibriated stress shapes and the principle of minimum complementary energy to efficiently estimate the magnitude of interlaminar stresses near the cut-out holes. Kassappogolu and Lagace [10], have essentially used the same method for obtaining analytical solutions for interlaminar stresses at free edges. Their assumed stress field, however, does not satisfy boundary conditions along the loaded edges. We have corrected this situation by assuming a stress field that satisfies boundary conditions along all the free edges.

Webber and Morton [11] described a method for obtaining analytical expressions for free edge stress fields due to thermal effects in a laminated composite plate. They have assumed a uniform temperature increase. They have attempted to obtain an analytical solution to this problem by using a complementary energy approach similar to that described by Kassappogolu and Lagace [10]. They have, however ignored the fact that the thermal expansion can take place in all directions. Interlaminar stresses are calculated by satisfying boundary conditions along only two directions. We also corrected this situation by assuming interlaminar stress fields that satisfy boundary

conditions along all the edges.

2.1 INTERLAMINAR STRESSES DUE TO MECHANICAL LOADING

In this analysis, we have considered cross ply laminates. A rectangular plate of dimension $2aX2bXh$ made from orthotropic layers, (0/90/0/90.....90/0), as shown in Figure 1, is considered. These layers are assumed to be symmetrically placed about the center plane of the plate. The plate is assumed to be subjected to an axial load of N_x. Using classical laminate plate theory, the stress field in the k th layer $\{\sigma\}^k$ can be determined. But these classical stresses do not satisfy the free surface stress free boundary conditions. To correct this situation, we should consider interlaminar stresses.

An approximate analytical solution has been obtained by assuming a stress field that satisfies equilibrium equations, all boundary conditions and interlaminar traction continuity conditions. The stress field is used to compute the complementary energy in the laminate. By taking the symmetry of the laminate into account, the assumed stress field in the range of $0 \leq x \leq a$ and $0 \leq y \leq b$ can be written as

$$\sigma_{xx}^k = \bar{\sigma}_{xx}^k + Ax[e^{-\phi_1 x} - e^{-\lambda\phi_1 x}] \tag{2.1}$$

$$\sigma_{yy}^k = \bar{\sigma}_{yy}^k[1 - e^{-\phi_2 y} - \phi_2 y e^{-\phi_2 y}] \tag{2.2}$$

$$\begin{aligned}\sigma_{zz}^k = {} & A[\phi_1 e^{-\phi_1 x}(\phi_1 x - 2) - \\ & \lambda\phi_1 e^{-\lambda\phi_1 x}(\lambda\phi_1 x - 2)] \\ & [\frac{z^2}{2} + zB_1^k + B_2^k] + \\ & \bar{\sigma}_{yy}^k \phi_2^2 e^{-\phi_2 y}[1 - \phi_2 y]\end{aligned} \tag{2.3}$$

$$[\frac{z^2}{2} + zD_1^k + D_2^k]$$

$$\sigma_{xz}^k = A[e^{-\phi_1 x}(1-\phi_1 x) - e^{-\lambda\phi_1 x} \quad (2.4)$$

$$(1-\lambda\phi_1 x)][z + B_1^k]$$

$$\sigma_{yz}^k = \bar{\sigma}_{yy}^k \phi_2^2 y e^{-\phi_2 y}[z + D_1^k] \quad (2.5)$$

where $\bar{\sigma}_{xx}^k$, and $\bar{\sigma}_{yy}^k$ are the classical laminate solutions [12]. In these equations, exponential functions [10] are used to account for the fact that interlaminar stresses reduce rapidly and the resulting stress field will be the classical laminate plate theory solution away from the free edges. The assumed solution satisfies the boundary condition and the equilibrium equations.

There are $4n$ constants $B_1^k, B_2^k, D_1^k, D_2^k$ for $k = 1, ..., n$. These constants are obtained to satisfy the interlaminar traction conditions similar to reference 10 but in two directions. They are

$$B_1^k = -\frac{1}{\sigma_{xx}^k}\sum_{j=1}^{k-1}\bar{\sigma}_{xx}^j t^j - z^k \quad (2.6)$$

$$B_2^k = \frac{1}{\sigma_{xx}^k}\sum_{j=1}^{k-1}\bar{\sigma}_{xx}^j t^j z^j - z^{k^2}/2 \quad (2.7)$$

$$D_1^k = -\frac{1}{\sigma_{yy}^k}\sum_{j=1}^{k-1}\bar{\sigma}_{yy}^j t^j - z^k \quad (2.8)$$

$$D_2^k = \frac{1}{\sigma_{yy}^k}\sum_{j=1}^{k-1}\bar{\sigma}_{yy}^j t^j z^j - z^{k^2}/2 \quad (2.9)$$

Constants ϕ_1, ϕ_2, λ and A are determined by minimizing the complementary energy for the laminate so that, the assumed stress field also leads to a compatible displacement field. The expression for the laminate complementary energy is given by the summation

$$\Pi_c = \sum_{k=1}^{n} \frac{1}{2} \int_v \int \int \sigma^T \bar{S} \sigma dV - \int_{Au} \int T u dA \tag{2.10}$$

Due to geometrical symmetry, only one fourth of the laminate is considered. It is assumed that the laminate is wide enough so that $e^{-a\phi_1}, e^{-a\phi_2}, e^{-b\phi_1}$ and $e^{-b\phi_2}$ are approximated to be zero. The second term in the integration is equal to zero since there is no prescribed displacement in the present problem. Four algebraic nonlinear coupled equations are obtained by taking partial derivatives of the expression for Π_c with respect to the four unknowns ϕ_1, ϕ_2, λ and A. By solving these four equations, $\phi_1, \phi_2, \lambda, A$ can be obtained.

2.2 INTERLAMINAR STRESSES DUE TO THERMAL LOADING

A cross-ply rectangular laminate plate of $2aX2bXh$ made from orthotropic layers,(0/90.....90/0), as shown in Figure 1 is considered. Each of the lamina in the plate is assumed to be subjected to a symmetric temperature change of ΔT^k. Using the classical laminate theory, classical stress field in k th layer is determined. To satisfy all the boundary conditions, the stress field is chosen as

$$\sigma_{xx}^k = \bar{\sigma}_{xx}^K [1 - e^{-\phi_1 x} - \phi_1 x e^{-\phi_1 x}] \tag{2.11}$$

$$\sigma_{yy}^k = \bar{\sigma}_{yy}^k [1 - e^{-\phi_2 y} - \phi_2 y e^{-\phi_2 y}] \tag{2.12}$$

$$\begin{aligned} \sigma_{zz}^k = {} & \bar{\sigma}_{xx}^k \phi_1^2 e^{-\phi_1 x} [1 - \phi_1 x] \\ & [\frac{z^2}{2} + z B_1^k + B_2^k] + \\ & \bar{\sigma}_{yy}^k \phi_2^2 e^{-\phi_2 y} [1 - \phi_2 y] \\ & [\frac{z^2}{2} + z D_1^k + D_2^k] \end{aligned} \tag{2.13}$$

$$\sigma_{xz}^k = \bar{\sigma}_{xx}^k \phi_1^2 x e^{-\phi_1 x}[z + B_1^k] \tag{2.14}$$

$$\sigma_{yz}^k = \bar{\sigma}_{yy}^k \phi_2^2 y e^{-\phi_2 y}[z + D_1^k] \tag{2.15}$$

where $\bar{\sigma}_{xx}^k$, and $\bar{\sigma}_{yy}^k$ are the classical laminate solutions. Symmetry of the laminate is taken into account. In these equations, exponential functions are used[10,11] to account for the fact that interlaminar stresses reduce rapidly and the resulting stress field will be the classical laminate plate theory solution away from the free edges. The assumed solution satisfy the boundary conditions.

There are $4n$ constants $B_1^k, B_2^k, D_1^k, D_2^k$ for $k = 1, ..., n$. These constants are obtained by satisfying the interlaminar traction conditions and are given by equations 6 to 9. Constants ϕ_1 and ϕ_2 are determined by minimizing the complementary energy for the laminate. The expression for the laminate complementary potential energy under thermal field is given by the summation

$$\Pi_c = \sum_{k=1}^{n} \frac{1}{2} \int_v \int \int \sigma^T \bar{S} \sigma dV + \int_v \int \int \sigma^T e_\theta dV - \int_{Au} \int T u dA \tag{2.16}$$

Again, due to geometrical symmetry, only one fourth of the laminate is considered. The third term in the integration is equal to zero since there is no prescribed displacement in the present problem. Two algebraic nonlinear coupled equations are obtained by taking partial derivatives of the expression for Π_c with respect to the two unknowns ϕ_1 and ϕ_2. By solving these two equations, ϕ_1, ϕ_2 can be obtained and as a result, all the stress filed can be obtained.

The objective of this report is to use the thermal loading as the actuation mechanism for the reduction of the interlaminar stresses. This actuation mechanism can be used for designing feedback controllers by using control theory.

2.3 NUMERICAL RESULTS

To study the accuracy of the assumed stress shapes, a rectangular laminate of CFRP AS-3201 with [0/90/90/0] orientation is considered. Material properties are E_{11} =139 GPa(20.2MPSI), E_{22} =11.7 GPa(1.7MPSI), G_{12} =5.8 GPa(0.85MPSI), μ_{12} =0.28. Interlaminar stress with the application of uniform axial stress is shown in Figure 2. Here the interlaminar stresses are shown near the free edge. x-location of the stresses are fixed at four times the thickness where as y location is varied from zero (free edge) to six times the thickness. It can be observed that the interlaminar stress reduces as we go away from the free edge. Dotted line in this figure denote the interlaminar stress estimation using reference 10. Now the x-location is changed to half the thickness and y-location is varied from zero to six times the thickness. Interlaminar normal stresses are shown in Figure 3. This location corresponds to the corner location of the plate. Objective for choosing this location is to study the effect of the unsatisfied boundary condition. Similar variation in the interlaminar stresses is observed between the results of the present approach and that of Reference 10.

To study the effect of unsatisfied boundary condition under thermal loading, we conducted similar studies. Keeping the x-location constant at four times the thickness, interlaminar stresses are plotted varying the y-location from zero to six times the thickness in Figure 4. Results are compared with the results of reference 11. Close agreement is seen between both the results. Now, x-location is changed to half the thickness. This location is close to the boundary in which boundary conditions have not been satisfied in reference 11. Interlaminar stresses are shown in Figure 5 as y location is varied. Significant difference is observed as we move away from the free edge. Results using the approach of reference 11 indicate stresses tend to become zero as we move away from the free edge where as results from the present approach are leading

to a constant value. This constant value is due to the interlaminar stresses near the second free boundary. To study the effect of this free boundary, we kept the location of y equal to 4 times the thickness and varied the location of x from zero (free edge) to four times the thickness. Results are shown in Figure 6. Results from the present approach show a large stress at the free edge and reduction in the stresses away from the edge. Results from reference 11 indicate zero interlaminar stresses erroneously. From this, we can conclude that the effect of unsatisfied boundary conditions under thermal loading is significant. Only region this effect is not significant is at the center of the plate.

To study the feasibility of applied thermal gradients, we considered the same rectangular laminate. By applying an axial load of 4375000 N/M (25,000 pounds/inch), interlaminar normal stresses developed at the interface of 0-90 is shown in Figure 7. In order to suppress these interlaminar stresses, we considered a temperature gradient of 25/0/0/25 (^{o}C) to suppress the interlaminar stresses. Interlaminar normal stress at the interface of 0-90 is shown in Figure 8. It can be seen from the Figures 7 and 8, that the applied thermal field resulted in exactly the same magnitude of interlaminar stresses in the opposite direction by making the effective interlaminar stresses equal to zero. Thus, by using the applied thermal field, we can reduce the high interlaminar stresses by controlling the formation and growth of delamination.

Chapter 3

EXPERIMENTAL VERIFICATION

To validate the developed theory, we initiated an experimental investigation with thermal actuators. Experimental techniques for measuring the interlaminar stresses by the use of piezoceramic transducer is first developed.

3.1 TEST SPECIMEN

A 0/90/0 glass epoxy specimen is fabricated using tow pregs supplied by Custom Composites Inc. of Atlanta, Georgia. The dimensions of the specimen are shown in Figure 9. Initially, three separate specimens are fabricated and bonded together, using epoxy resin with embedded piezoceramic transducers for measurement of interlaminar stresses and a thin film of nichrome wire for thermal loading. The thickness of the piezoceramic transducer is 0.0006 inch and the thickness of the nichrome wire is 0.0001 inch. Another piezoceramic transducer is bonded to the upper surface of the specimen for calibration. Dimensions of the overall specimen meet the ASTM standard of Tensile testing [13].

3.2 INSTRUMENTATION

The piezoceramic transducers bonded to the specimen act as sensors. Terminals of the piezoceramic sensor are attached, through a charge amplifier, to a digital oscilloscope. The embedded nichrome wire is connected to a thermal controller for applying the thermal loading. The instrumentation diagram is shown in Figure 10. The mechanical loading is applied through an INSTRON 8501. Since the piezoceramic sensors can not detect a steady load, it was decided to apply a cyclic load of very low frequency that is of the order of 1/2 Hz for mechanical loading and thermal loading. This frequency is significantly below the first harmonic frequency of the beam but above the cutoff frequency of the oscilloscope, at which PZT sensor can detect without errors.

From analysis, it can be shown that when mechanical load is applied, interlaminar stresses can be identified from voltage measurements

$$\sigma_{zz} = \frac{V^2 - V^1}{K_{23} h} \tag{3.1}$$

Here V_1 is the voltage measured by the sensor that is bonded to the surface and V_2 is the voltage measured by the embedded sensor. K_{23} is a function of the piezoceramic material constant and h is the thickness of the layer of the laminate. Similarly, for the specimen that is subjected to thermal loading, interlaminar stresses can be obtained as

$$\sigma_{zz} = \frac{V^2 - V^1 - f(T)}{K_{23} h} \tag{3.2}$$

Here $f(T)$ is the correction term to account for the different coefficient of thermal expansion of the laminate and thermal effect on transducers.

3.3 TESTS

Experiments were conducted and interlaminar stresses were determined from the recorded data using appropriate caliberation. Tests were separately conducted under mechanical loading and under both the mechanical and thermal load. The effect of mechanical loading on the interlaminar stress is shown in Figure 11. It can be seen that there is an increase in the interlaminar stress with the increase in the mechanical loading. Magnitudes were compared with analytical results for accuracy.

Results of effect of thermal loading is shown in Figure 12. A mechanical cyclic loading of 0-100 lbs is applied and a thermal loading of 0-15 degree farenheit is applied. The interlaminar stress that was observed to be positive when the mechanical loading is applied is observed to be negative when this thermal loading is applied in addition to the mechanical load indicates that interlaminar tension is changed to interlaminar compression by the application of a relatively small thermal field. The results presented here should be as considered only preliminary. More experiments should be conducted to establish the trend and the amplitude of actual control effort that is needed.

Chapter 4

CONCLUSIONS

Interlaminar stresses are determined under axial mechanical loading and under combined axial mechanical and thermal loading. Feasibility of applied thermal gradients as the actuation mechanism for the reduction of the magnitude of interlaminar stresses has been analytically demonstrated. Preliminary experimental investigation validates analytical studies.

ACKNOWLEDGEMENTS

This work was supported by a grant to the Center of Excellence for Computational Modeling of Aircraft Structures from the Federal Aviation Administration.

REFERENCES

[1] Pagano, N.J. and Pipes, R.B., " Some Observations on the Interlaminar strength of composite Laminates", Int.J.Mech. Sci., Vol 15,(1973), pp 679-688.

[2] Pagano, N.J. and Lackman, L.M.," Prevention of Delamination of composite laminates", AIAA Jl Vol.13, 1975,pp 399-401.

[3] Mignery, L.A., Tan, T.M., and Sun, C.T., " The Use of Stitching to Suppress Delamination in Laminated Composites", ASTM Symposium on Delaminations and Debonding of Materials, 1983.

[4] Chan, W.S., Rogers, C. and Aker,S., " Improvement of Edge Delamination Strength of Composite Laminates Using Adhesive Layers", Composite Materials: Testing and Design, ASTM STP 893, 1986.

[5] Chan, W.S., Rogers, C., Cronkhite, J.D and Martin, J, " Delamination Control of Composite Rotor Hubs", Journal of helicopter Society, pp 60-69, 1986.

[6] Rogers, C.A., Liang, C., Li, S,, " Active Damage Control of Hybrid Material Systems Using Induced Strain Actuators", Proc. 32 SDM Conference, pp 1190-1199, 1991.

[7] Hanagud, S., Nagesh Babu, G.L , Roglin, R. and Savanur, S., "Active Control of Delaminations in composite structures" Proc. 33rd AIAA/ASME/ASCE/AHS SDM Conference, pp 1819-1830, 1992.

[8] Gummadi, Lakshmana Nagesh Babu, "Active Control of Delaminations in

Smart Composite Structures", Ph.D Thesis presented to school of Aerospace Engineering, Georgia Institute of technology, Atlanta, December 1992.

[9] Nishioka, T. and Atluri, S.N., " Stress Analysis of Holes in Angle- Ply Laminates: An efficient Assumed Stress 'Special - Hole Element' Approach and a simple estimation method", Computers and Structures, Vol. 15, No. 2, 1982, pp 135-147.

[10] Kassapoglou, C. and Lagace, P.A., " An Efficient Method for the Calculation of Interlaminar Stresses in Composite Materials", Journal of Applied Mechanics, Vol 53, 1986, pp 744- 750.

[11] Webber, J.P.H and Morton, S.K., " An Analytical Solution for the Thermal Stresses at the Free Edges of Laminated Plates", Composite Science and Technology, 1993.

[12] Tsai, S.W., " Composites Design", Think Composites, Dayton, 1987.

[13] ASTM Standard D3039 -76 " Standard Test Method for Tensile Properties of Fiber Resin Composites", American Society for Testing and materials, 1993.

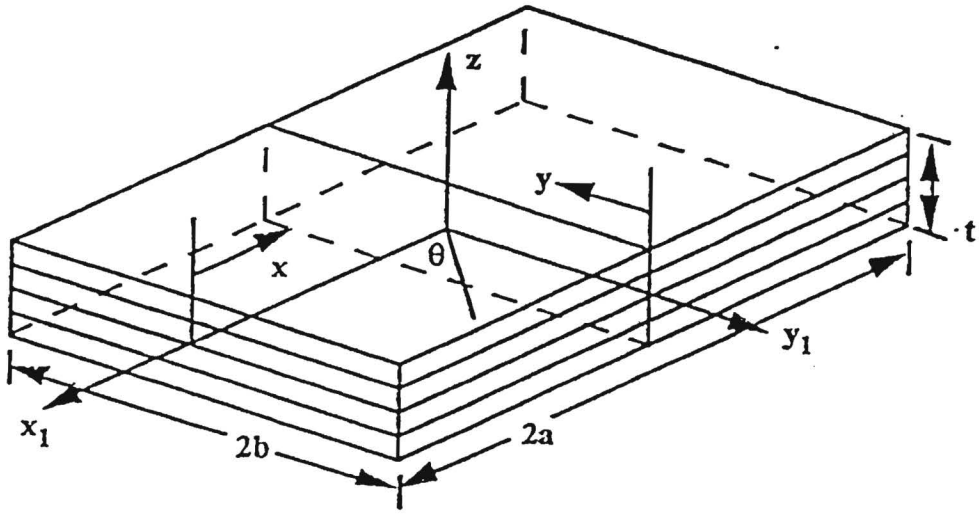

Figure 1: Laminated plate geometry

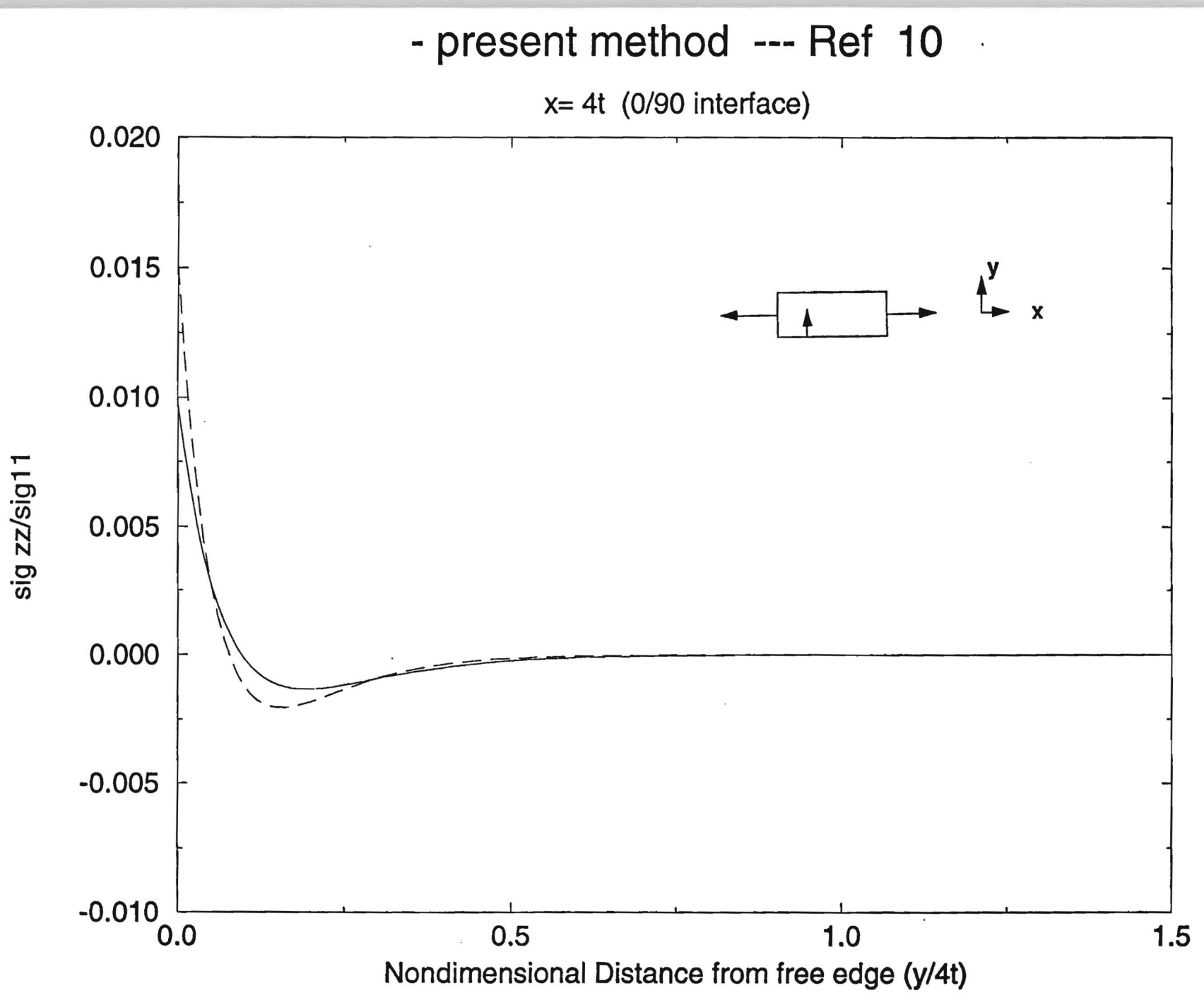

Figure 2: Variation of σ_{zz} due to mechanical load (x=4t)

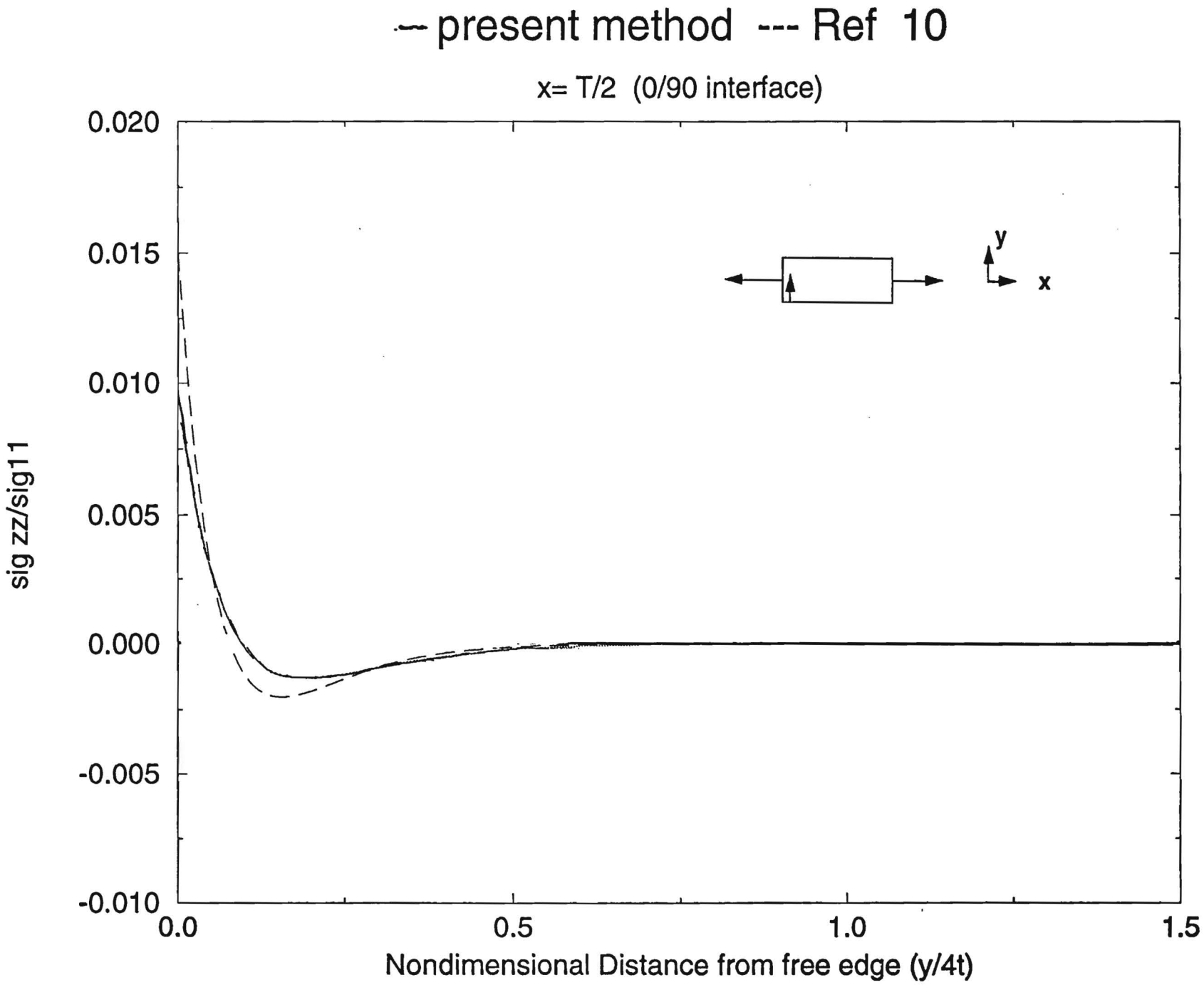

Figure 3: Variation of σ_{zz} due to mechanical load (x=t/2)

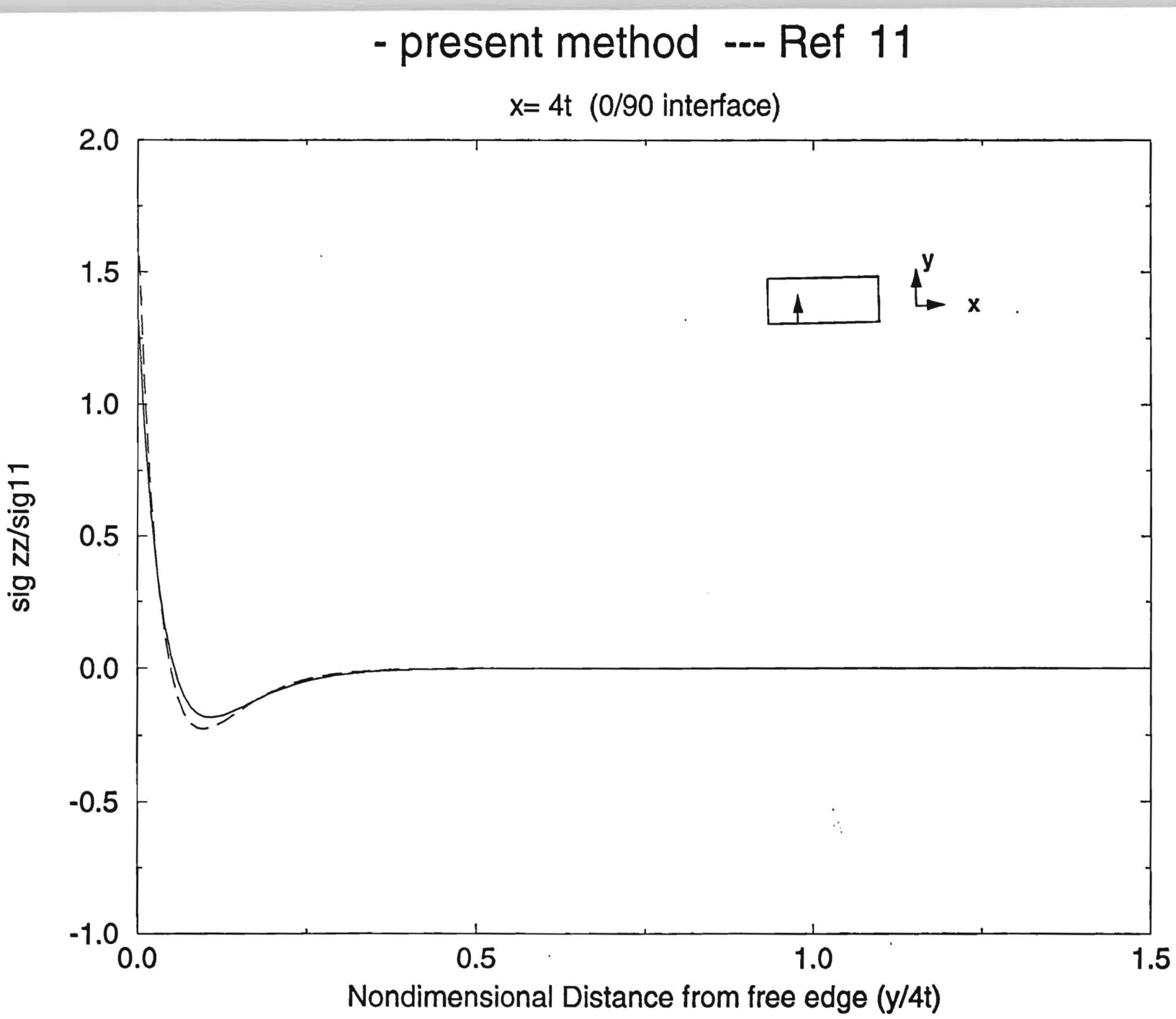

Figure 4: Variation of σ_{zz} due to thermal load (x=4t)

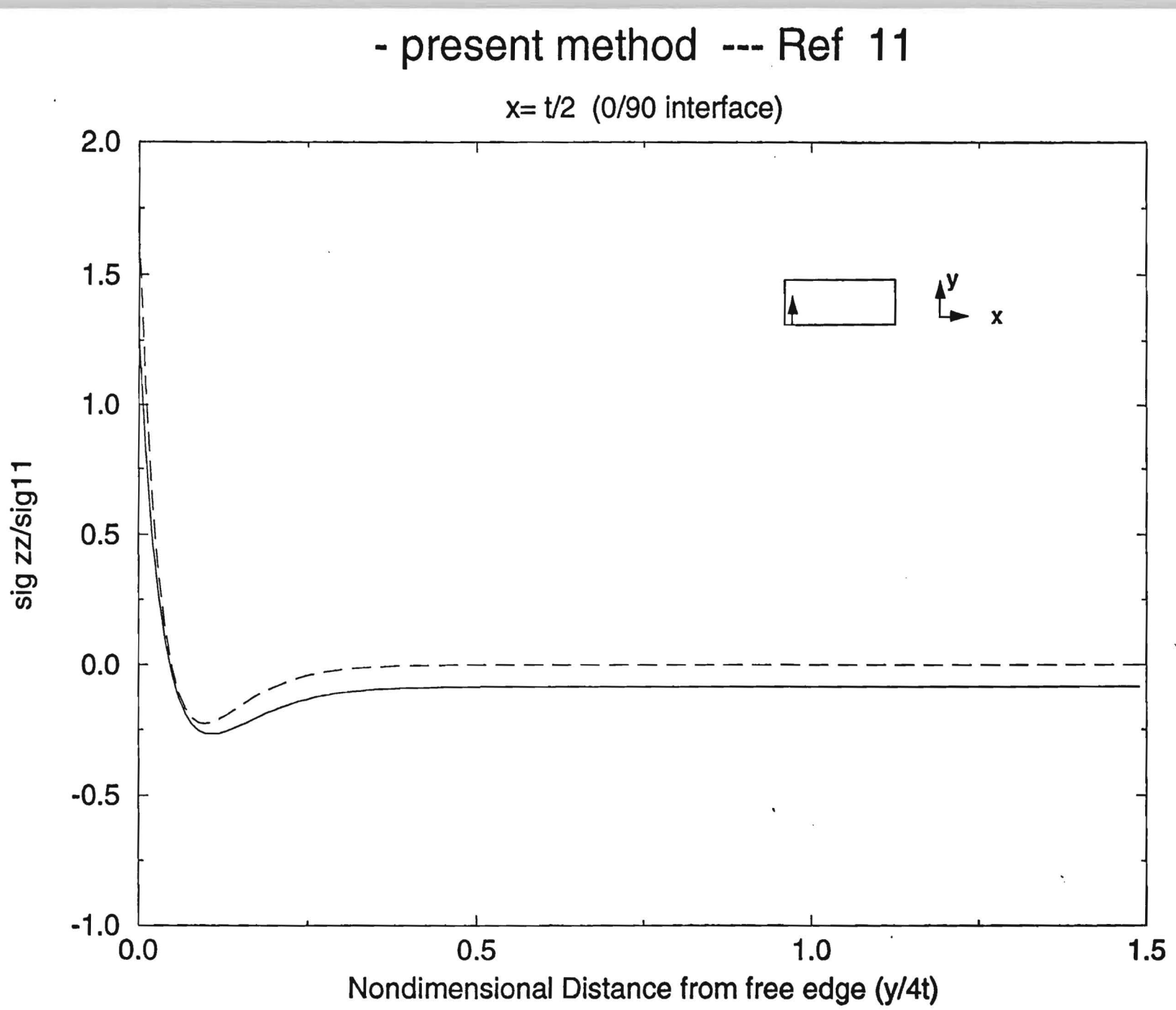

Figure 5: Variation of σ_{zz} due to thermal load (x=t/2)

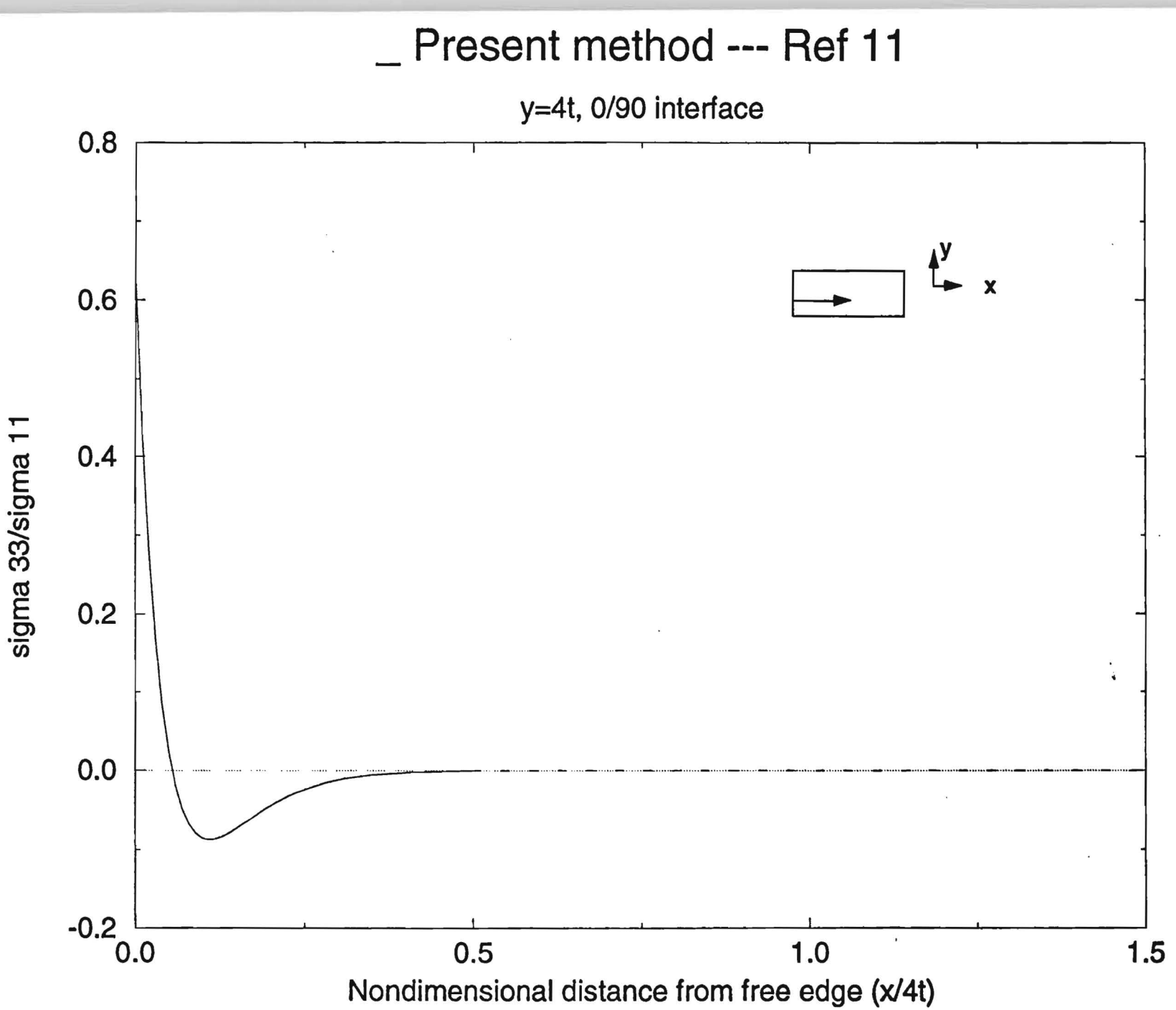

Figure 6: Variation of σ_{zz} due to thermal load (y=4t)

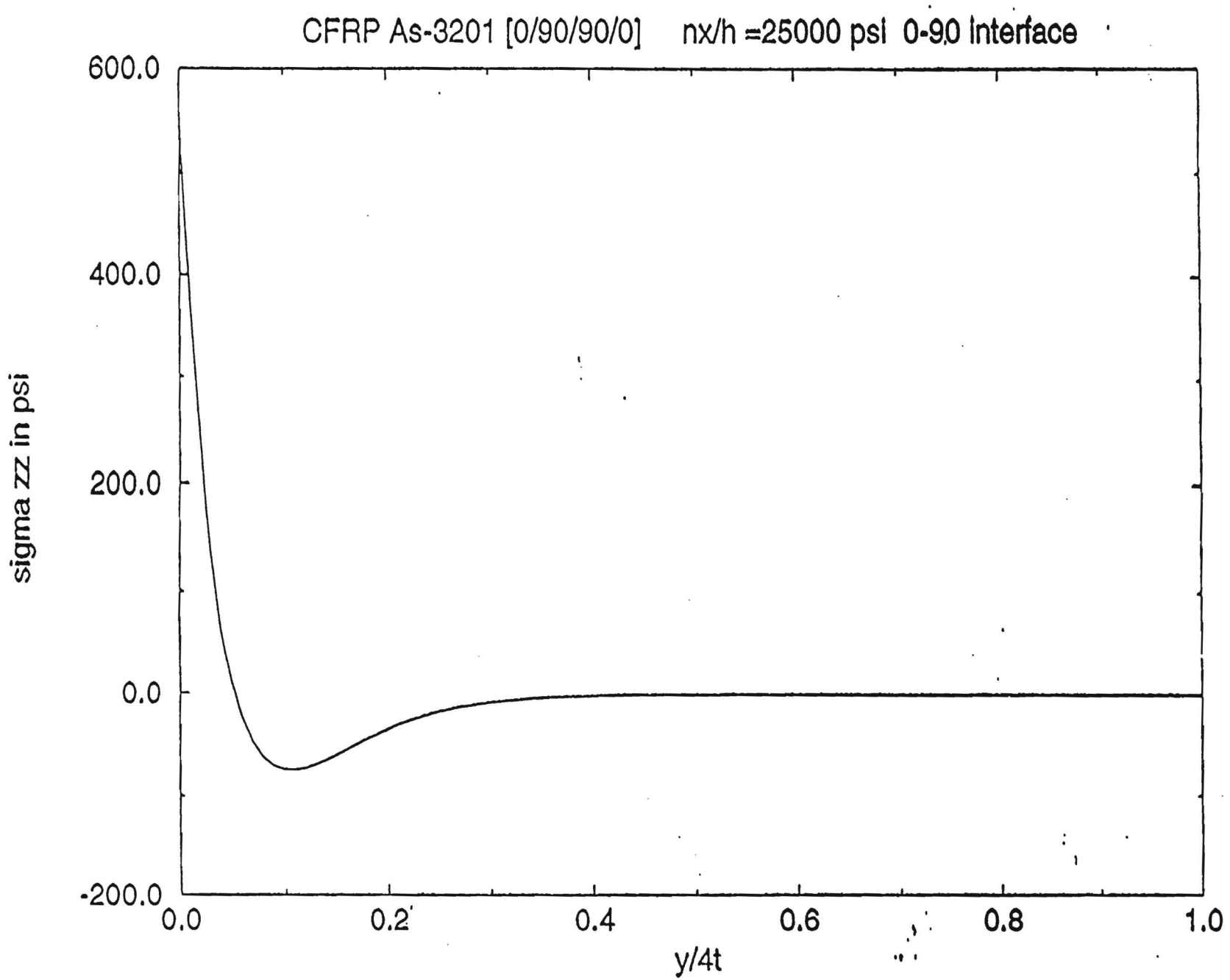

Figure 7: σ_{zz} **Distribution due to Mechanical Loading**

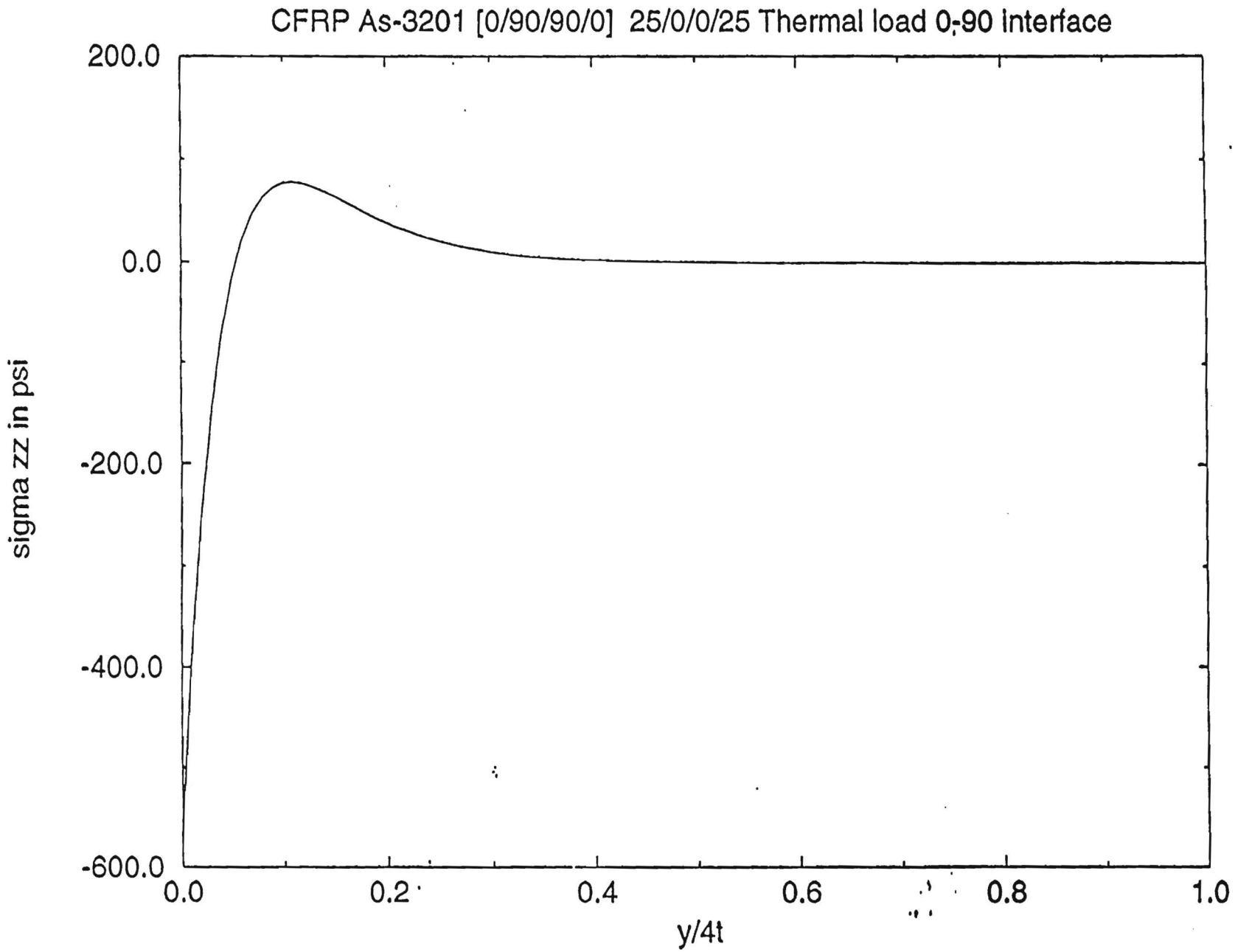

Figure 8: σ_{zz} Distribution due to Thermal Loading

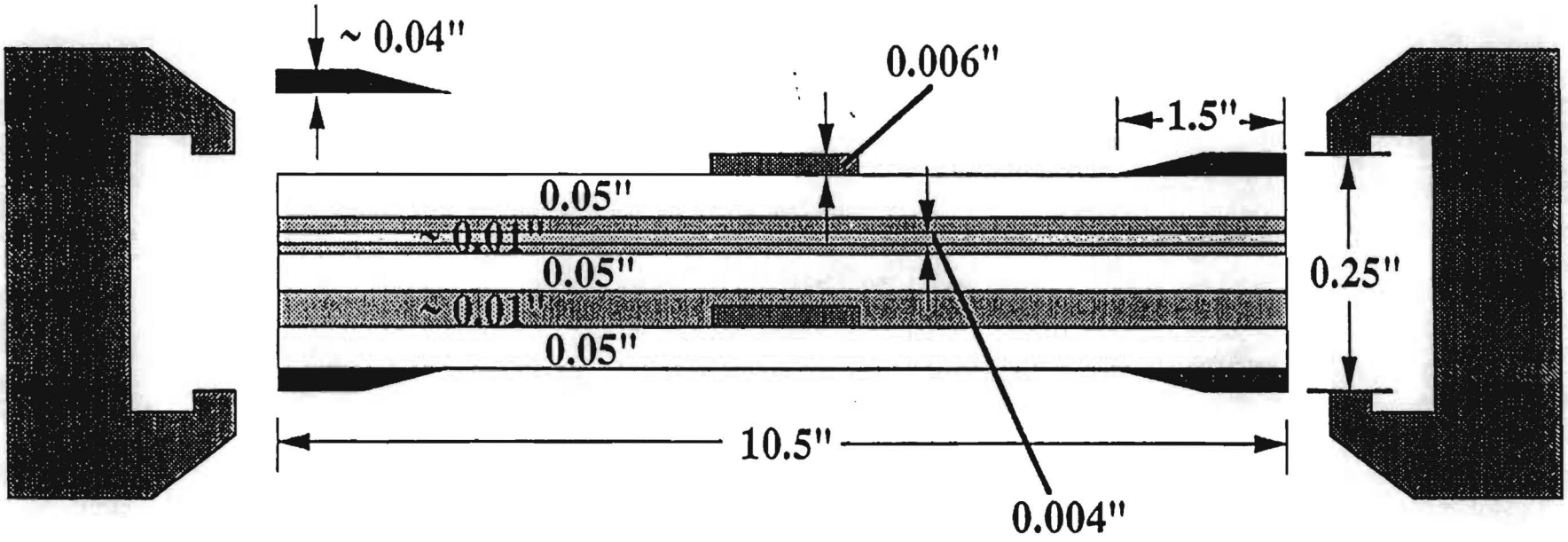

Specimen is 1"in width

Piezo sensors are 2.25" long by .2" wide
and are placed at the free edges

Figure 9: Specimen dimensions

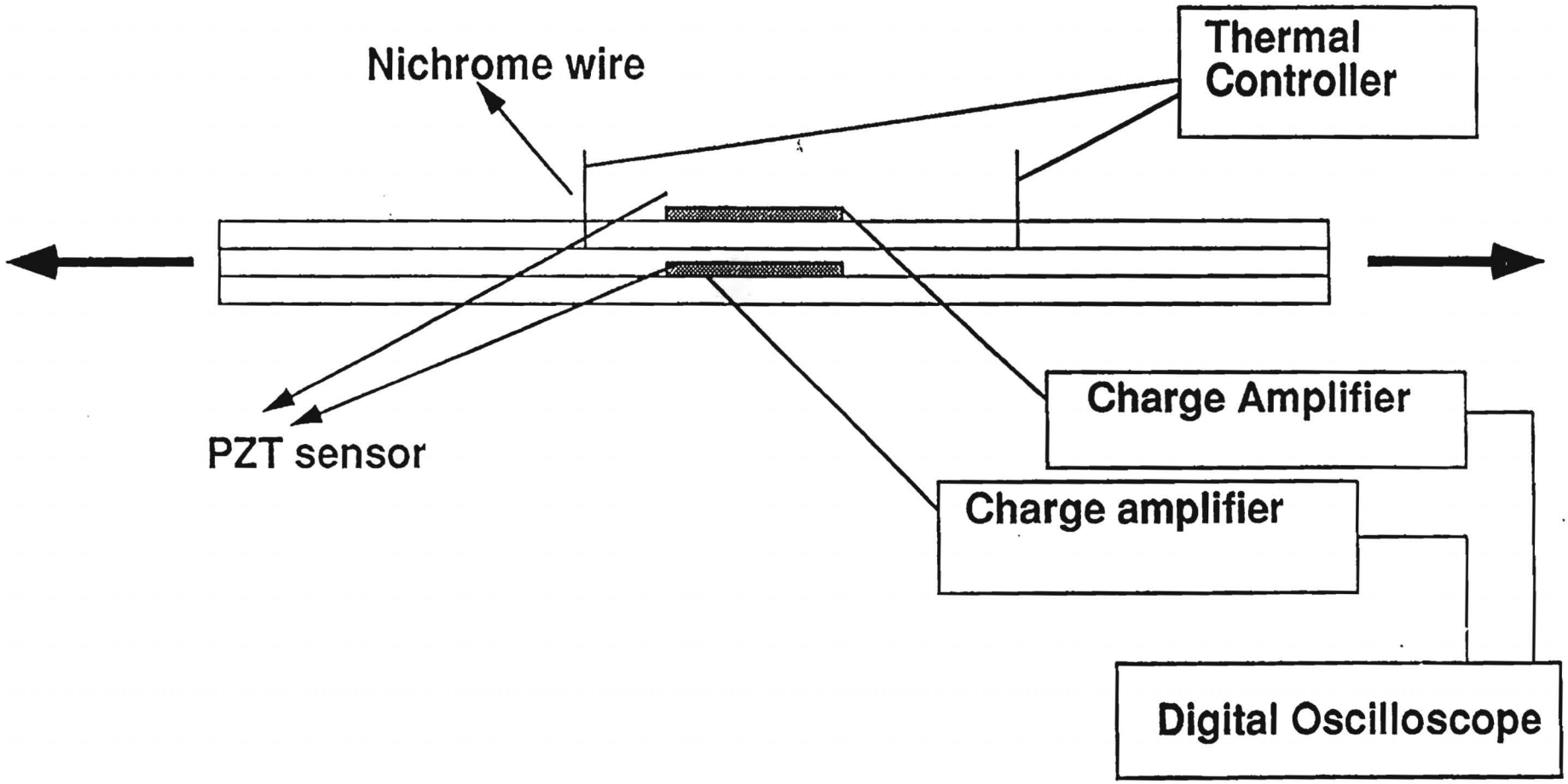

Figure 10: Experimental setup

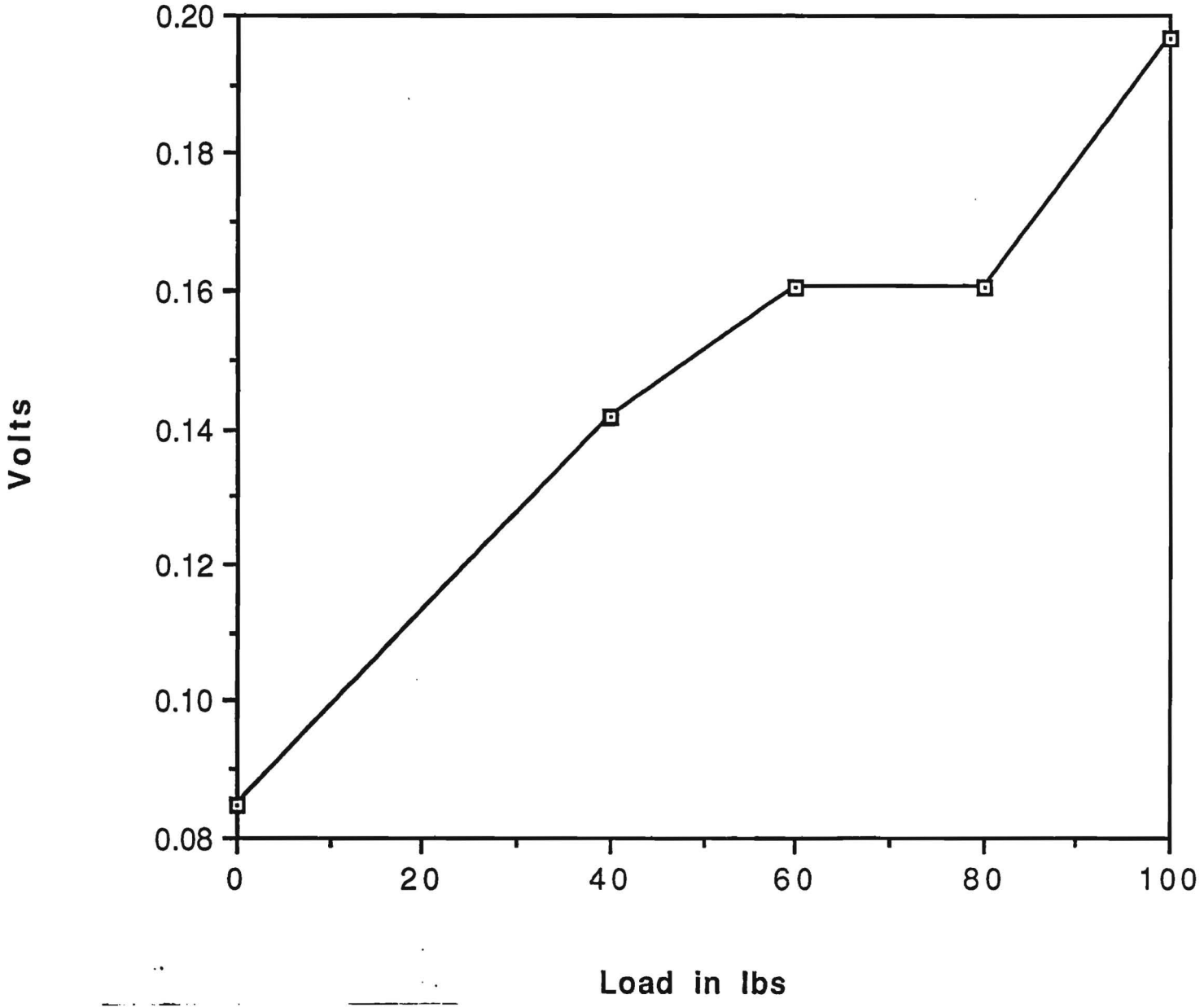

Figure 11: Interlaminar stresses due to mechanical load (σ_{zz})

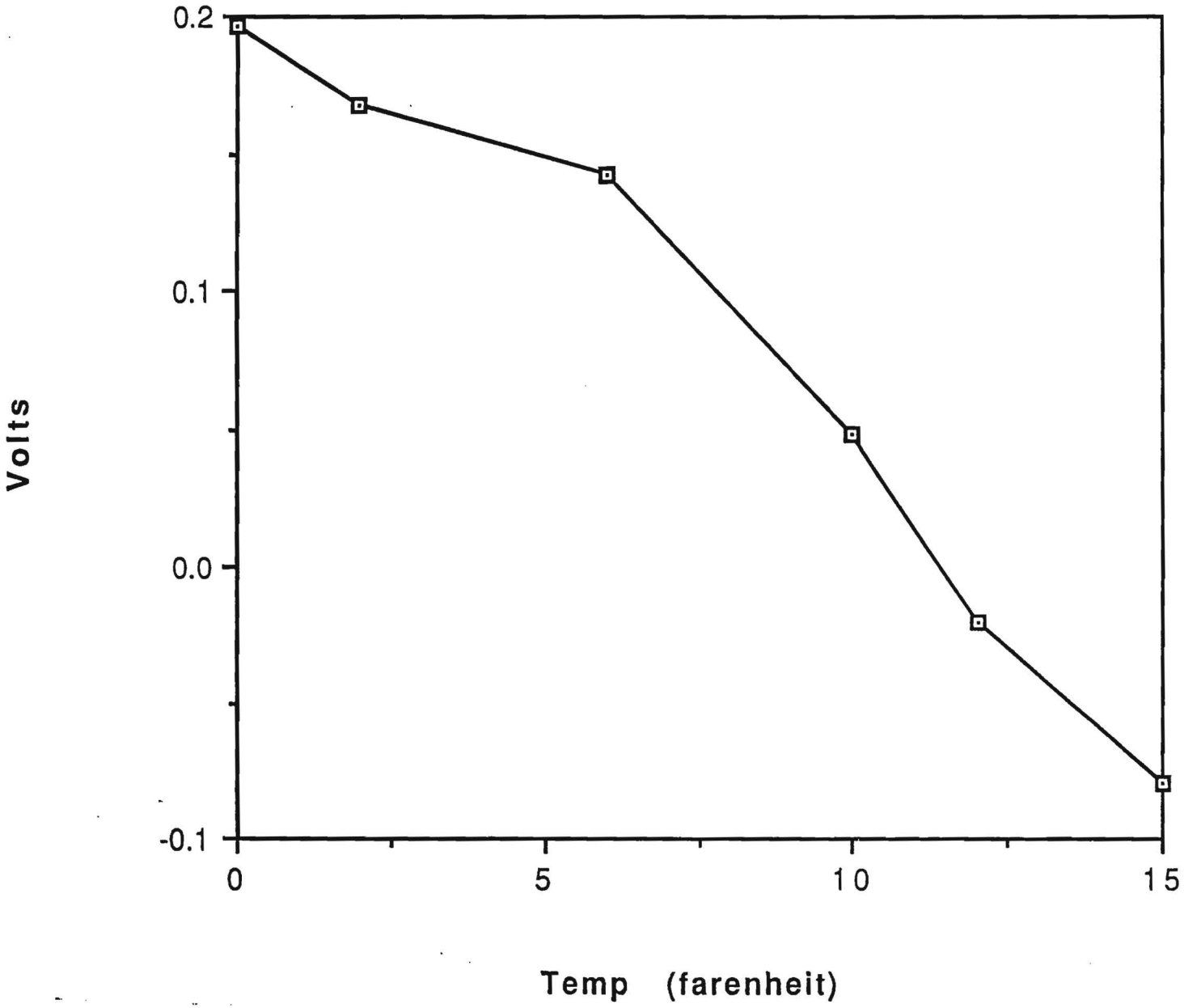

Figure 12: Interlaminar stresses due to mechanical and thermal loading (σ_{zz})

A Methodology for Computing Nonlinear Fracture Parameters for a Bulging Crack in a Pressurised Aircraft Fuselage

V. B. Shenoy, D. O. Potyondy, and S. N. Atluri

FAA Center of Excellence
for
Computational Modeling of Aircraft Structures
Georgia Institute of Technology
A. French Building
Atlanta, GA 30332-0356

March 1994

A Methodology for Computing Nonlinear Fracture Parameters for a Bulging Crack in a Pressurised Aircraft Fuselage

Vijay B. Shenoy* David O. Potyondy† Satya N. Atluri‡

Computational Modeling Center, Georgia Institute of Technology,
Atlanta, GA 30332-0356, USA

Abstract

A computational methodology for obtaining nonlinear fracture parameters which account for the effects of plasticity at the tips of a bulging crack in a pressurised aircraft fuselage is developed. The methodology involves a hierarchical three stage analysis (global, intermediate, and local) of the cracked fuselage, with the crack incorporated into the model at each stage. The global analysis is performed using a linear elastic shell finite element model in which the stiffeners are treated as beam elements. The geometrically nonlinear nature of the bulging phenomenon is emulated in the intermediate analysis using a geometrically nonlinear shell finite element model. The local analysis is a three-dimensional solid finite element model of the cracked skin using a hypoelastic-plastic rate formulation. Kinematic boundary conditions for each stage are obtained from the preceeding stage in the hierarchy using a general mesh independent mechanism. The T^* integral, which accounts for both large deformations and plasticity, is taken to be the fracture parameter characterising the severity of the conditions at the crack tip, and is evaluated from the local analysis using the Equivalent Domain Integral(EDI) method. The implementation of the EDI technique for finite deformations in shell space is also outlined. The methodology is applied to a number of example problems for which correction factors relating the nonlinear T^* values to those obtained from a linear elastic stiffened shell analysis are computed. The issue of flapping is addressed by investigating the behaviour of the longitudinal stress parallel to the crack for various cases.

*Graduate Research Assistant
†Postdoctoral Fellow
‡Institute Professor & Regents' Professor of Engineering

1 Introduction

Aircraft structures experience fatigue loading which may lead to Widespread Fatigue Damage (WFD). The aircraft must be tolerant to the cracks thus formed. Assessment of damage tolerance may be achieved by full-scale testing combined with computational analyses. Full-scale testing is expensive, cumbersome, and dangerous (due to the possibility of explosive decompression). It is thus imperative that computational methods are developed so that the required number of experiments can be reduced.

Large longitudinal cracks in fuselage skins are often formed by the coalescence of many smaller cracks as in the case of Multiple Site Damage (MSD). The crack growth is driven by the fatigue loading arising from internal pressurisation of the fuselage shell during each flight. Such cracks may control the residual strength of the structure. Analysis of such cracks is complicated by the bulging deformation of the crack edges. (A large deformation analysis is required to obtain the correct displacements.) For a crack of sufficient length, the longitudinal stress in the immediate vicinity of the crack tip may equal or exceed a certain critical value. As a consequence, the crack may change its growth direction from longitudinal to circumferential, a phenomenon known as flapping. Flapping is a favorable phenomenon in that it prevents the explosive decompression of the aircraft by relieving the internal pressure and thereby stopping the crack growth. Thus, a knowledge of the stress field around the tip of such a crack is essential for the economic design of new aircraft and the structural integrity evaluation of aging aircraft. Computational tools are needed to achieve this goal. The computational problems associated with large longitudinal cracks in pressurised fuselages are thus twofold: (1) obtain the values of a suitable fracture parameter that quantifies the severity of the conditions near the crack tip; and, (2) obtain a quantitative criteria for flapping (cf. Atluri and Tong (1991)).

The stress field near the crack tip is affected by various factors viz. the large deformation, presence of stiffeners and other structural elements, and plasticity near the crack tip. Previous work has ignored the plasticity effects and utilized the stress intensity factor as the fracture parameter. The bulging of the crack edges leads to an increase in the mode-I stress intensity factor from that of an equivalent flat sheet and can be expressed in terms of a "bulge factor". Swift (1987) obtained an empirical formula for the bulge factor by comparison of fatigue test results of full-scale DC-10 fuselage panels with those of flat panels. Swift's factor was found to be valid for cracks that were sufficiently far away from the stiffeners. Lemaitre, Turbat, and Loubet (1977) were the first to perform large deformation analysis of

these problems and obtained the energy release rate. Riks (1987) performed a geometrically nonlinear analysis to obtain energy release rates which were used to determine bulge factors. In addition, he found that the bulging displacement at the center of the crack is a nonlinear function of the pressure and that the bulge factor decreases with increasing internal pressure, thereby demonstrating the importance of a geometrically nonlinear analysis. Ansell (1988) performed a geometrically nonlinear analysis and reported deformation patterns similar to those reported by Riks. He also performed a large number of experiments, and parametric studies, and proposed an empirical formula for the bulge factor. Chen (1990) and Chen and Schijve (1991) have also developed empirical formulae for bulge factors. Their analysis was performed on a simplified model of the zone of bulge, using an energy balance approach and an expression for the out-of-plane displacement based on experimental observations. Rankin, Brogan, and Riks (1993) have developed a computational procedure to evaluate the energy release rates of cracks in pressurised fuselages based on geometrically nonlinear shell finite elements. They used a "crack-closure integral" approach to determine the energy release rate.

Other workers have computed stress intensity factors or energy release rates directly for particular configurations. Miller, Kaelber, and Worden (1992) computed stress intensity factors for cracks in narrow-body and wide-body configurations using a geometrically nonlinear finite element analysis and found good comparison of fatigue life predictions made using these stress intensity factors with results of full-scale pressurised panel tests. Potyondy (1993) developed a methodology for simulating curvilinear crack growth in thin, stiffened, pressurised shells and a modified crack closure integral for computing various components of the energy release rate from the results of a geometrically nonlinear shell finite element analysis. He obtained good comparison of crack trajectory and fatigue life with results of a full-scale pressurised panel test.

It is worth noting again that the plasticity at the crack tip has been ignored completely in all previous work. The present work describes a computational methodology which incorporates the plasticity effects and allows one to compute a suitable nonlinear fracture parameter, the T^*-integral, that is valid in the presence of the large deformations and plasticity occurring near the crack tip. The methodology consists of a hierarchical modeling of the cracked fuselage involving three stages of analysis. The first (global) is a linear shell finite element analysis of a large portion of the fuselage; the second (intermediate) is a geometrically nonlinear shell finite element analysis of a smaller portion (the section in which bulge effects are predominant); and, the third (local) is a hypoelastic-plastic three-dimensional solid finite

element analysis of the fuselage skin. In Section 2, we describe the theoretical formulation of each stage and the software framework that links together all of the stages. A critical evaluation of the fracture parameters is presented in Section 3, where it is pointed out that conventional LEFM fracture parameters are not theoretically valid for this class of problems, and the use of certain nonlinear fracture parameters (Atluri (1982)) is suggested. The T^*-integral is evaluated from the equilibrium state using the Equivalent Domain Integral (EDI) method. Section 4 contains the results of example problems that demonstrate the effectiveness of the methodology.

2 Computational Methodology

The present methodology involves a hierarchical modeling of the cracked fuselage. The software framework is presented along with the theoretical formulations of the various stages of the analysis. We begin with a description of the hierarchical modeling strategy.

2.1 Hierarchical Modeling Strategy

The problem of crack bulging is a localised nonlinear phenomenon restricted to a few bays adjacent to the crack. A hierarchical strategy allows the accurate computation of the nonlinear fracture parameters without requiring an excessive computational effort. The hierarchical strategy is designed so that the factors affecting pertinent behaviour are well approximated at an appropriate stage in the analysis. For the modeling of the bulging phenomenon, we propose the use of a three-stage (global, intermediate, and local) modeling strategy. Each succeeding stage in the hierarchy accounts for more complex behaviour occurring over a smaller portion of the fuselage structure. In this hierarchical strategy, the global analysis models the general behaviour of the cracked fuselage, the intermediate model captures the geometrically nonlinear aspect of the bulging deformation, and the local analysis accounts for both the geometrically and materially nonlinear behaviour. Cracks are incorporated into all three models. Each model is loaded by the internal pressure and gets its kinematic boundary conditions from the preceeding model in the hierarchy.

The three models in the hierarchical strategy are illustrated in Fig. 1. The first stage (global model) is a linear elastic shell finite element analysis in which the stiffeners are modeled using beam elements. A linear model suffices, since global buckling and related

instability phenomena are not investigated. Symmetry boundary conditions approximating a closed cylinder are imposed on the global model. The portion of the fuselage containing the crack, where the nonlinear bulging is prominent, is contained within the geometrically nonlinear shell finite element model which forms the second stage (intermediate model) of the analysis. Stiffeners are modeled using shell elements. Displacements and rotations from the global model are imposed on the panel boundary. The third stage (local model) is a 3D solid finite element analysis of a portion of the cracked skin. The portion is chosen so that the plastic zone is contained well within its boundary. Displacements and rotations from the intermediate model are imposed on the portion's boundary after transformation from the shell space to 3D. A hypoelastic-plastic constitutive model is used with an objective stress update. The nonlinear fracture parameters are evaluated from the local model.

2.2 Global Analysis

The global analysis models the general behaviour of the cracked fuselage accounting for stress redistribution caused by the presence of the crack and the stiffeners. It is performed in shell space, invoking the Kirchhoff-Love kinematic assumptions and the theory of linear elasticity. The principle of minimum potential energy is used to obtain the following equation of equilibrium:

$$\begin{aligned} \Pi(\mathbf{u}) &= \int_V W(\boldsymbol{\epsilon}) dV - \int_{\partial V^\sigma} \mathbf{t} \cdot \mathbf{u} dS \\ \delta\Pi &= 0 \end{aligned} \tag{1}$$

where Π is the potential energy, W is the strain energy density, $\boldsymbol{\epsilon}$ is the strain tensor, $\mathbf{t}$ are the prescribed tractions, and $\mathbf{u}$ are the displacements which must satisfy the essential (kinematic) boundary conditions. On invoking the Kirchhoff-Love assumptions, one obtains a linear variation of the strain tensor $\boldsymbol{\epsilon}$, through the thickness in terms of the in-plane strains $\epsilon_{\alpha\beta}$, and the bending strains $\kappa_{\alpha\beta}$. The strain energy density W, may be written as

$$W(\boldsymbol{\epsilon}) = \frac{1}{2}\left[hC^{\alpha\beta\gamma\delta}\epsilon_{\alpha\beta}\epsilon_{\gamma\delta} + \frac{h^3}{12}C^{\alpha\beta\gamma\delta}\kappa_{\alpha\beta}\kappa_{\gamma\delta} \right],$$

where

$$C^{\alpha\beta\gamma\delta} = \frac{E}{1-\nu^2}\left[\nu a^{\alpha\beta}a^{\gamma\delta} + \frac{1-\nu}{2}\left(a^{\alpha\delta}a^{\beta\gamma} + a^{\alpha\gamma}a^{\beta\delta} \right) \right],$$

$C^{\alpha\beta\gamma\delta}$ is the elasticity tensor, $a^{\alpha\beta}$ is the metric tensor of the middle surface, h is the shell thickness, E is the Young's modulus, and ν is the Poisson's ratio.

A finite element version of the above variational principle is used to obtain the equilibrium solution. A four-noded cylindrical shell element with five degrees of freedom per node (three displacements and two rotations), developed by Ashwell and Sabir (1972), is used for the fuselage shell discretisation. This is a quasi-conforming type of element in which an independent variation of strains is assumed. A general rigid motion involving six undetermined parameters is obtained upon solving the differential equations resulting from equating the strains to zero. Fourteen other parameters are used to discretise the strains, which are made to satisfy some simplified versions of the compatibility conditions. These expressions for strains are now integrated to obtain the displacements, and the rigid motion is added. The twenty undetermined parameters are now expressed in terms of the twenty undetermined nodal degrees of freedom. The strains, expressed in terms of these twenty quantities, are used in Eq. (1).

In the global analysis, stiffeners are modeled as beam elements (the variational principle of Eq. (1) is used *mutatis mutandis*). Compatibility of stiffener and shell displacements is ensured by developing the stiffener elements by degenerating the shell element. Cracks are incorporated into the global analysis model as unconnected nodes belonging to the elements adjacent to the crack. The crack tip singularity is not modeled explicitly, since the plasticity occurring near the crack tip will be modeled in the local analysis. Also, the size of the global model is chosen so that the effects of the crack are not felt at the boundary. As noted above, a linear global analysis suffices if one is not interested in modeling global buckling and related instability phenomena.

2.3 Intermediate Analysis

The intermediate analysis models the geometrically nonlinear behaviour of the cracked fuselage in the region where the bulging phenomenon occurs. The principle of virtual work is used to obtain the following equation of equilibrium:

$$\int_V (\mathbf{C} : \mathbf{E}) : \mathbf{E}(\delta\mathbf{u}) dV - \int_{\partial V^\sigma} J\mathbf{F}^{-1}\mathbf{t} \cdot \delta\mathbf{u} dS = 0 \tag{2}$$

where $\mathbf{C}$ is the elasticity tensor, $\mathbf{E}$ is the Green-Lagrange strain tensor, $\mathbf{F}$ is the gradient of deformation with

$$\mathbf{E} = \frac{1}{2}(\mathbf{F}^T \cdot \mathbf{F} - \mathbf{I})$$

$$J = det(\mathbf{F}), \tag{3}$$

$\mathbf{t}$ are the prescribed tractions in the deformed configuration, and $\delta\mathbf{u}$ must satisfy the essential kinematic boundary conditions. The integration in Eq. (2) is performed upon the undeformed configuration (Total Lagrangian type formulation). In the bulging problem, the principle of virtual work (Eq. (2)) does not reduce to a minimum potential energy principle because of the non-conservative nature of the pressure loading. Under the Kirchhoff-Love assumptions, a linear through-thickness variation of the Green-Lagrange strain is obtained in terms of the in-plane strains and the bending strains of the middle surface (cf. Koiter (1966)). (Eq. (2)), after integrating through the thickness and expressing all quantities in shell variables, is used as the basis of the finite element formulation.

In the intermediate analysis, both stiffeners and skin are modeled using a four-noded quadrilateral shell element with drilling degrees of freedom (cf. Rankin and Brogan (1991)). This element formulation employs an incompatible displacement field with a cubic variation of the bending field and a linear/cubic variation of the inplane field, resulting in six degrees of freedom per node (three displacements and three rotations). The rigid motion is removed from the total displacement field using an element level co-rotational procedure (Nour-Omid and Rankin (1991), and references therein). The solution of the resulting nonlinear finite element equations is achieved through the Riks arc-length control algorithm (Riks (1984, 1987a)). Convergence is checked using the norms of the residual load and displacement vectors, and the energy norm.

2.4 Local Analysis

The local analysis models the plastic behaviour as well as finite deformation of the skin near the crack tip to enable the computation of the nonlinear fracture parameters. A finite-deformation hypoelastic-plastic 3D solid finite element formulation is adopted to model a small portion of the cracked skin. Nonlinear boundary value problems of this type are solved using incremental procedures. Various forms of incremental methods have been proposed, with the Total Lagrangian (TL) and Updated Lagrangian (UL) being prominent. Atluri (1980) has derived several general variational principles for classical finite strain elasto-plasticity in both TL and UL forms. An Updated Lagrangian scheme with an objective stress update algorithm is used for the present analysis. For the sake of clarity, we describe the formulation from first principles.

The basic difficulty associated with finite deformation problems is that the final deformed configuration is not known *a priori*. Various stress and strain measures which express the dynamical state and deformation, respectively, have been developed in both the reference configuration (usually the undeformed configuration) and the deformed configuration. For a succinct summary of various stresses, strain measures, equilibrium equations, etc., cf. Atluri (1984). The Updated Lagrangian strategy uses the incremental motion to update the configuration, i.e., the incremental displacement solution obtained in the current step is added to the current coordinates, and the reference configuration for the next step is chosen to be the new configuration thus obtained.

The equilibrium equation of the deformed configuration with respect to any reference configuration may be written in terms of the first Piola-Kirchhoff stress tensor $\mathbf{T}$, as

$$\nabla_{\mathbf{X}} \cdot \mathbf{T} = \mathbf{0}, \tag{4}$$

where ∇ is the gradient operator, $\mathbf{X}$ denotes the reference coordinates, and body forces are taken to be zero. The constitutive model is a hypoelastic-plastic model that is a generalisation of the classical rate independent plasticity (viscous behaviour of all orders are imagined to be absent, cf. Hill (1968)). A rate formulation is thus a natural platform for posing the boundary value problem. The rate is understood to be with respect to a monotonic pseudo-time parameter or a load parameter. (For the class of problems discussed herein, the internal pressure of the fuselage is a natural candidate for this parameter.) Noting that the body in question is in equilibrium at every instant, we may write an equilibrium equation for the rates (cf. Hill (1968)) as

$$\nabla_{\mathbf{X}} \cdot \dot{\mathbf{T}} = \mathbf{0}, \tag{5}$$

where $(\dot{})$ is the material time derivative. Assuming $\delta\mathbf{v}$ to be a velocity field that satisfies the essential velocity boundary conditions, the following equation can be obtained from Eq. (5)

$$\int_V \left(\nabla_{\mathbf{X}} \cdot \dot{\mathbf{T}}\right) \cdot \delta\mathbf{v} dV = 0. \tag{6}$$

Integrating Eq. (6) by parts (Gauss divergence theorem) leaves

$$\int_V \dot{\mathbf{T}} : \nabla_{\mathbf{X}} \otimes \delta\mathbf{v} dV - \int_{\partial V^\sigma} \dot{\mathbf{t}} \cdot \delta\mathbf{v} dS = 0, \tag{7}$$

where $\dot{\mathbf{t}}$ is the prescribed traction rate. Eq. (7) is the rate analog of the principle of virtual work and forms the basis for the incremental finite element formulation presented here.

Eq. (7) is a general expression for rate equilibrium that shall be specialised for the Updated Lagrangian strategy and the hypoelastic-plastic constitutive relation. Assume that the time parameter varies in the range $[0, \Lambda]$. We seek equilibrium states corresponding to a finite number of instances $\{0, \lambda_1, ..., \lambda_i, ..., \Lambda\}$. Consider now a generic stage i, in the process, for which all stresses and internal variables are known. We wish to reach state $i+1$. In the Updated Lagrangian strategy, the equilibrium configuration i, is used as the reference configuration for the step going from i to $i+1$. Eq. (7) may be rewritten as

$$\int_{V_i} \dot{\mathbf{T}} : \nabla_{\mathbf{x}_i} \otimes \delta\mathbf{v} dV - \int_{\partial V_i^\sigma} \dot{\mathbf{t}} \cdot \delta\mathbf{v} dS = 0. \tag{8}$$

Noting that the current configuration is the reference configuration, we have the following identities (cf. Atluri (1980)):

$$\begin{aligned} \mathbf{L} \equiv \nabla \otimes \mathbf{v}, \quad \mathbf{D} &= sym(\mathbf{L}), \quad \mathbf{W} = asym(\mathbf{L}), \\ \dot{\mathbf{T}} &= \boldsymbol{\sigma}^\circ - \mathbf{D}\boldsymbol{\tau} + \boldsymbol{\tau}\mathbf{D} - \boldsymbol{\tau}\mathbf{L}, \end{aligned}$$

where $\mathbf{D}$ is the rate of deformation tensor, $\mathbf{W}$ is the spin tensor, $\boldsymbol{\tau}$ is the Cauchy stress tensor, $\boldsymbol{\sigma}$ is the Kirchhoff stress tensor, and $\boldsymbol{\sigma}^\circ$ is the Jaumann rate of Kirchhoff stress

$$\boldsymbol{\sigma}^\circ = \dot{\boldsymbol{\sigma}} - \mathbf{W}\boldsymbol{\sigma} + \boldsymbol{\sigma}\mathbf{W}. \tag{9}$$

Eq. (8) now becomes

$$\int_{V_i} (\boldsymbol{\sigma}^\circ - \mathbf{D}\boldsymbol{\tau} + \boldsymbol{\tau}\mathbf{D} - \boldsymbol{\tau}\mathbf{L}) : \delta\mathbf{L} dV - \int_{\partial V_i^\sigma} \dot{\mathbf{t}} \cdot \delta\mathbf{v} dS = 0. \tag{10}$$

The material is assumed to obey a hypoelastic-plastic constitutive law of which we present a brief discussion. The development of this constitutive equation is an attempt to generalise the Prandtl-Reuss equations of the flow theory of classical plasticity. Since these rules are in terms of rates, an elastic constitutive equation for finite deformation involving rates is required. Truesdell (1955) developed a "rate-elasticity" (hypoelasticity) in his attempt to construct an elastic behaviour which did not have a natural state. Truesdell's formulation reads

$$\mathcal{L}(\boldsymbol{\sigma}) = f(\mathbf{D}),$$

where $\mathcal{L}()$ is an objective rate that renders the constitutive equation objective. All constitutive equations must satisfy the Principle of Objectivity (Truesdell and Noll (1965)) which

is felt like a *cantus firmus* in all of continuum mechanics. Note that $\mathbf{D}$ depends only on the current state and is independent of any chosen reference configuration. Assuming f to be a linear homogeneous function, and taking the objective rate to be the Jaumann rate, linear hypoelasticity is obtained as

$$\begin{aligned} \boldsymbol{\sigma}^{\circ} &= \mathbf{C} : \mathbf{D} \\ C_{ijkl} &= \frac{E}{1+\nu}\left[\delta_{ik}\delta_{jl} + \delta_{il}\delta_{jk} + \frac{2\nu}{1-2\nu}\delta_{ij}\delta_{kl}\right]. \end{aligned} \tag{11}$$

The Jaumann rate coincides with the Green-Nagdhi rate (given that the reference configuration is the current configuration), which is a special type of Lie-derivative in which the rotation tensor is used to perform the pull-back and push-forward operation on the stress. Physically, the Jaumann rate simply "checks for a change in the Mohr circle(s)", i.e., if the principal stresses at a material point do not change, the Jaumann rate vanishes at that point. For this formulation, linear hypoelasticity is assumed to represent the elastic behaviour.

A generalisation of Eq. (11) to include a plastic flow rule is obtained as follows (Hill (1968)). Assume an additive split of the rate of deformation tensor into elastic and plastic parts as

$$\mathbf{D} = \mathbf{D}^e + \mathbf{D}^p \tag{12}$$

where $\mathbf{D}^e$ and $\mathbf{D}^p$ represent the elastic and plastic parts, respectively. Assuming a von Mises type yield condition, and a Prandtl-Reuss type flow rule one obtains (Wang and Atluri (1994))

$$\begin{aligned} \boldsymbol{\sigma}^{\circ} &= \mathbf{C}^{ep} : \mathbf{D}, \\ \mathbf{C}^{ep} &= \mathbf{C} - \frac{3a^2}{2\left(\frac{2}{3}h(\gamma) + a\right)\bar{\sigma}^2}\boldsymbol{\sigma}' \otimes \boldsymbol{\sigma}', \end{aligned} \tag{13}$$

where h is the slope of the uniaxial stress strain curve, γ is the effective plastic strain, $\bar{\sigma}$ is the effective stress, $\boldsymbol{\sigma}'$ is the deviator, and

$$\begin{aligned} \gamma &= \int_0^t \sqrt{\frac{2}{3}\mathbf{D}^p : \mathbf{D}^p}\, dt, \\ \bar{\sigma} &= \sqrt{\frac{3}{2}\boldsymbol{\sigma}' : \boldsymbol{\sigma}'}, \\ a &= \frac{E}{1+\nu}. \end{aligned} \tag{14}$$

On using Eq. (13) in Eq. (10)

$$\int_{V_i} (\mathbf{C}^{ep} : \mathbf{D} - \mathbf{D}\boldsymbol{\tau} + \boldsymbol{\tau}\mathbf{D} - \boldsymbol{\tau}\mathbf{L}) : \delta\mathbf{L} dV - \int_{\partial V_i^{\sigma}} \dot{\mathbf{t}} \cdot \delta\mathbf{v} dS = 0 \tag{15}$$

is obtained. This equation is used to generate the incremental finite element equations, the solution of which give the incremental nodal displacements. We note here that for the bulging problem, Eq. (15) is not equivalent to the rate potential principle due to the non-conservative nature of the live pressure loading; thus, a computation with very large load steps may lead to an erroneous equilibrium state.

Once the incremental displacements are available, the stresses corresponding to these displacement increments must be evaluated. A stress update algorithm is incrementally objective (Rubenstein and Atluri (1983)) in that a rigid incremental motion of the body should produce zero incremental stresses. We use, here, the algorithm developed by (Rubenstein and Atluri (1983)) which involves the computation of the rotation tensor $\mathbf{R}$, from the computed spin tensor $\mathbf{W}$, via

$$\mathbf{R} = \exp(\mathbf{W}\Delta t) = \mathbf{I} + \frac{\sin(\omega\Delta t)}{\omega}\mathbf{W} + \frac{(1 - \cos(\omega\Delta t))}{\omega^2}\mathbf{W}^2 \tag{16}$$

where ω is the Euclidian norm of the rotation vector (angular velocity) corresponding to the spin tensor $\mathbf{W}$. The present stress $\boldsymbol{\sigma}$, and the rate of deformation $\mathbf{D}$, are rotated using the rotation $\mathbf{R}$, and the incremental stress corresponding to the incremental deformation is obtained. The total stress (the sum of the rotated stress and the computed stress increment) is rotated back using $\mathbf{R}$, and the new stress state is obtained. The computation of the incremental stress corresponding to the incremental deformation is achieved by the Radial Return algorithm of which we do not present the details (cf. Nikishkov and Atluri (1994); Wang and Atluri (1994)).

In the local analysis, a small portion of the cracked skin is discretised using 20-noded brick elements, with a single layer of elements through the thickness. The computational procedure may be summarised as follows. The load vector corresponding to the step-increment is obtained. The stiffness matrix is computed, and the incremental displacements are obtained. The objective stress update algorithm is used to integrate the rate constitutive equation and obtain the incremental stresses corresponding to the incremental displacements. After an update of configuration, a residual load vector is evaluated, and the process is continued with the residual vector taken as the forcing vector until the residual load vector, in norm, is less than a prescribed tolerance. The process is continued until the desired load level is reached.

2.5 Software Framework

The hierarchical modeling strategy integrates the three computational models whose theoretical formulation was described above. The software implementation consists of three independent analysis codes linked via a general mechanism for mapping information between them. The analysis codes are executed sequentially (global, intermediate, then local) with each generating the generalized displacement field that serves as the kinematic boundary conditions along the boundaries of the succeeding model.

The boundary conditions that must be transferred between the three models are described in the following with the aid of Fig. 2. In this Figure, the shell surface and boundary of model-i are denoted by S_i and ∂S_i, respectively, where the subscripts 0, 1, and 2 refer to the global, intermediate, and local models. In addition to the live pressure loading applied to the skin of each model, the kinematic boundary conditions for the intermediate and local models are described by

$$\mathbf{u}_1 = \lambda \mathbf{u}_0(\mathbf{x}), \mathbf{x} \in \partial S_1 \tag{17}$$

$$\mathbf{u}_2 = \mathbf{u}_1(\mathbf{x}, \lambda), \mathbf{x} \in \partial S_2 \tag{18}$$

where $\mathbf{u}_i$ is the generalized displacement for model-i, and λ is the load factor for the nonlinear analyses. Note that the generalized displacements of the intermediate model are functions of λ .

2.5.1 Mapping Information Between Analysis Models

A mechanism for associating vector field information with arbitrary surfaces is described. It allows the boundary conditions of Eqs. (17-18) to be mapped between models in a mesh independent fashion, e.g., the mesh of the intermediate model in S_1 need not contain element edges that lie along ∂S_2. Each point on the surface is associated with a specific value of the vector field by providing a mapping function, whose input consists of the surface point (query point) and whose output consists of the value of the vector field at that point. ($\mathbf{u}_0$ in Eq. (17) is an example of such a mapping function in which $\mathbf{x}$ is the query point.) The mapping function is implemented as a software object called a Mesh RePresentation (MRP) that employs a nonlinear search algorithm and contains all information necessary to support it.

The MRP information consists of a surface mesh, of 2D and/or 1D elements, that describes both the field variation and the surface geometry. Determining the field value at a given query point is a two step process. First, the point on the mesh nearest (in Cartesian space) to the query point is found. Next, the element's shape functions are evaluated at the local element coordinates of this point, and are used to interpolate the field value from the element nodal values. Note that a search is made for the nearest point to a given query point, thereby allowing for the possibility that the query point may not lie exactly on the mesh. Such cases arise because of differing approximate representations of the underlying surface.

Finding the point on the surface mesh nearest to a given query point is a geometric search requiring that the nearest point within each element of the mesh be found. The search for the nearest point within an element will, in general and depending upon the shape functions, require a nonlinear procedure. A Newton-Raphson iteration is used. The search proceeds by first finding the closest point on each element edge. For 1D elements, the search is now complete. For 2D elements, if the query point is above the element, the closest point that lies within the element surface (excluding its boundary) is found. The first step involves a one parameter Newton-Raphson search over each edge whereas the second step involves a two parameter Newton-Raphson search over the element's interior. Details of the search algorithm can be found in Potyondy (1993).

The MRP-object supports a geometry based query of a static vector field. It can be extended to support a geometry based query of a time-varying vector field using a software object called a Temporal MRP (TMRP). The TMRP implements a mapping function, whose input consists of a query point *and* a time value and whose output consists of the value of the vector field at that point and time. ($\mathbf{u}_1$ in Eq. (18) is an example of such a mapping function in which $\mathbf{x}$ is the query point and λ is the temporal value.)

The TMRP information consists of a collection of MRP-objects, each of which is associated with a unique value of λ. The two MRP-objects whose λ values bracket the given λ are found, and each is queried for the field value at the given query point $\mathbf{x}$. The returned vector field value $\mathbf{v}$, is linearly interpolated by

$$\begin{aligned} \mathbf{v}(\mathbf{x},\lambda) &= \mathbf{v}(\mathbf{x},\lambda_0)[1-s] + \mathbf{v}(\mathbf{x},\lambda_1)[s] \\ s &= \frac{\lambda-\lambda_0}{\lambda_1-\lambda_0} \end{aligned} \tag{19}$$

$$\lambda_0 \leq \lambda \leq \lambda_1$$

where $\mathbf{v}(\mathbf{x}, \lambda_i)$ comes from the MRP-object associated with λ_i.

2.5.2 Software Components and Interaction

The three independent analysis codes consist of SOFRAC (Singh, Park, and Atluri (1994)) for the global analysis, STAGS (Almroth, Brogan, and Stanley (1986)) for the intermediate analysis, and FPS (presently developed) for the local analysis. In addition, FRANC3D (Potyondy (1993); Gray, Potyondy, Lutz, Wawrzynek, Martha, and Ingraffea (1994)) provides a geometry based modeling environment and interface to the STAGS code. Also, the MRP and TMRP software objects described in the preceeding section provide the mechanism for transferring the boundary conditions of Eqs. (17-18) between the three analysis models.

The steps required to obtain the final equilibrium state for the local model are now described. 1) The SOFRAC model is constructed and analyzed to obtain the equilibrium state of the global model. The generalized displacements along ∂S_1 are extracted and placed into a MRP file containing 1D elements. 2) The STAGS model is constructed within FRANC3D using the information in the MRP file. The STAGS model is analyzed to obtain the equilibrium state of the intermediate model. The generalized displacements within S_1, for each load factor for which an equilibrium state was computed during the nonlinear analysis, are extracted and placed into a TMRP file containing 2D elements. 3) The FPS model is constructed and analyzed to obtain the final equilibrium state of the local model. During the analysis, the generalized displacements along ∂S_2 are obtained by querying the TMRP information and employing Kirchhoff assumptions to map the generalized displacements, that include rotation components, into applied displacements along the faces of the corresponding solid elements.

3 Fracture Parameters

Conventional fracture mechanics (small-strain, linear elastic) states the rather remarkable fact that the state of stress near a crack tip is governed by a single parameter (consisting of three components in the general case) which has come to be known as the stress intensity

factor (SIF). Much of the fracture mechanics has evolved around these factors. The strength of the singularity near the crack tip in a linear elastic flat plate can be characterised by stress intensity factors with separate SIFs for inplane and bending stresses (Hui and Zehnder (1993), and references therein). For curved shells, in general there are no solutions available. The conventional approach in modeling long cracks in curved shells has been to perform a flat plate analysis of the crack in an osculating plane with the crack tip. The well known HRR (Hutchinson (1968); Rice and Rosengren (1968)) solution insists that the stress field around an elasto-plastic crack (assuming deformation theory of plasticity) is governed by the celebrated J-integral.

All of the above parameters are based upon a small-strain assumption and the linear equations of equilibrium making their theoretical validity questionable when applied to the bulging problem which is a geometrically nonlinear phenomenon. The use of stress intensity factors (or the conventional J-integral) is clearly not theoretically justifiable (Lemaitre, Turbat, and Loubet (1977)). Several other points may also be noted. The stress intensity factors of the linear theory are derived using the linear equations of equilibrium (in the linear theory, there exists the class of statically determinate problems), and it is not necessary that the same behaviour is obtained in the nonlinear regime (there are no statically determinate problems, all quantities of an equilibrium state depend on the material behaviour). Lemaitre *et al.* suggested the use of the energy release rate as a fracture parameter. Various components of the energy release rate were computed by Rankin, Brogan, and Riks (1993). Riks (1987), Ansell (1988), and Potyondy (1993) also computed the energy release rate, or components thereof, and obtained stress intensity factors using relations derived from the linear theory. Note that all of these analyses were elastic.

Atluri (1982, 1986) has obtained several parameters valid for finite deformations and plasticity. A valid fracture parameter for finite deformations and plasticity is the T^*_ϵ-integral defined as

$$\begin{aligned} T^*_{\epsilon\alpha} &= \int_{\Gamma_\epsilon} (W n_\alpha - n_i T_{ij} u_{j,\alpha})\, dA \\ \alpha &= 1, 2. \end{aligned} \tag{20}$$

The "1" direction is the direction of the crack tip (longitudinal in the case of the cracks discussed here, cf. Fig. 3), the "2" direction is normal to the crack line (circumferential), Γ_ϵ is a vanishingly small cylindrical contour surface of radius ϵ around the crack tip, n_i is

a normal to the above contour, T_{ij} is the first Piola-Kirchhoff stress, u_j is the displacement vector, and W is the stress work density

$$W = \int_0^t \boldsymbol{\sigma} : \mathbf{D} dt. \tag{21}$$

The T^*-integral is valid for a general 3D crack. It is evaluated using the Equivalent Domain Integral (EDI) method developed by Nikishkov and Atluri (1987), which has proven to be a robust method for obtaining energy-flux based fracture parameters. This procedure consists of rewriting $T^*_{\epsilon\alpha}$ in Eq. (20) using an arbitrary continuous function s, which vanishes on a far-field contour Γ and is unity on Γ_ϵ :

$$\begin{aligned} T^*_{\epsilon\alpha}\Delta &= \int_{\Gamma_\epsilon} (W n_\alpha - n_i T_{ij} u_{j,\alpha})\, s dA - \int_\Gamma (W n_\alpha - n_i T_{ij} u_{j,\alpha})\, s dA \\ &= -\int_{V-V_\epsilon} \left[\frac{\partial}{\partial X_\alpha}(Ws) - \frac{\partial}{\partial X_i}\left(T_{ij} \frac{\partial u_j}{\partial X_\alpha} s \right) \right] dV \end{aligned} \tag{22}$$

where $V - V_\epsilon$ is the volume enclosed between Γ and Γ_ϵ, and Δ depends on the s-function and the thickness of the domain (cf. Nikishkov and Atluri (1987)). The advantage of this method is that the integration is carried out on a finite volume domain (not a vanishingly small surface), and this lends numerical stability to the computation. The integral in Eq. (22) is evaluated in the limit as ϵ tends to zero at the equilibrium state obtained for the local model.

4 Example Computations

The present methodology was exercised on a number of example problems. The bulging of cracks is affected by many factors such as the presence of stiffeners, fastener flexibility, and skin thickness. In the present examples, fastener flexibility is not modeled; the skin is assumed to be attached rigidly to the stiffeners. (Note that fastener flexibility could be modeled by incorporating it into the global and intermediate models.) The example fuselage model is representative of the narrow-body fuselage configuration studied by Rankin, Brogan, and Riks (1993) (cf. Fig. 4 and Table 1). The effects of stiffening elements, crack length, crack location, and skin thickness are examined for the eight cases shown in Table 2. The offset value in Table 2 is the distance by which the crack has been offset from the midbay towards the stringer (in the positive X_2 direction of Fig. 3).

The Young's modulus of the skin and the stiffeners are 10,500 ksi and 10,700 ksi, respectively. The Poission's ratio for both skin and stiffeners is taken to be 0.33. For the local analysis of the skin, a piecewise approximation of the uni-axial stress strain curve of Al2024-T3, given in MIL-HDBK-5E (1987), is adopted for the flow rule (cf. Table 3).

The global model consisted of 5 frame bays and 7 stringer bays with symmetry boundary conditions approximating a closed cylinder. Each of the eight finite element models contained approximately 12,000 degrees of freedom. The intermediate model consisted of 2 frame bays and 3 stringer bays (a slightly larger intermediate model was required for Case 2 since the bulge out zone was considerably larger), with an average of approximately 15,000 degrees of freedom. The local analysis was performed on a rectangular portion of the skin with a side length of 5-6 inches with approximately 8,000 degrees of freedom. For the computation of the T^*-integral, the s-function was chosen to be constant through the thickness (type (d) function of Nikishkov and Atluri (1987)), with sixteen elements about the crack tip used in the computation. The total analysis time did not exceed eight hours (global: 0.4-0.5 hours; intermediate: 1.5-2.0 hours; local: 3-5 hours) on a HP-735 workstation. Deformed meshes of the various stages of the analysis for Case 6 are shown in Figs. 5, 6, and 7. As expected, the global model significantly overestimates the bulging deformation which is modeled more accurately in the intermediate and local models.

The computed values of T^* are presented in Figs. 8, 9, 10, and 11. In most cases, plasticity began to develop after a load factor of 0.25, and at large load factors (greater than 0.5) the variation of T^* is nearly linear. Stiffening produces a large reduction in T_1^* (cf. Fig. 8). Offsetting the crack by one quarter of bay length has no significant effect on T_1^* (cf. Fig. 9). Doubling the skin thickness while maintaining the same loading, reduces T_1^* by more than half (cf. Fig. 10). The computed value of T_2^* is negligible for the cases in which the crack is centered between the stringers and becomes nearly 40% of the T_1^* value for the offset crack (cf. Fig. 11).

In an industrial setting, a nonlinear analysis may not be feasible, and often only a linear stiffened shell analysis is performed. The present methodology can be used to develop correction factors which account for both the geometric nonlinearity and the plasticity. The correction factors are defined as

$$\text{Correction Factor} = \frac{T_1^*}{T_{1l}^*}, \tag{23}$$

where T_{1l}^* denotes the value of T_1^* obtained from a linear elastic analysis. Note that T_{1l}^* is

identical to the energy release rate G_l, and is related to the various stress intensity factors via well-known relations (cf. Hui and Zehnder (1993)).

The computed correction factors are presented in Figs. 12 and 13. They were obtained by performing a geometrically linear elastic analysis of the intermediate model and computing G_l using the extension of the modified crack closure technique described in Potyondy (1993). The correction factors decrease as the load is increased because of the growing discrepancy between the bulging displacements of the linear and nonlinear models. As the nonlinear effects increase with increasing load factor, the correction factor decreases. The trend in the correction factors for the thicker shell differs from that of the thinner cases (cf. Fig. 13). The nonlinear effects do not develop as rapidly for the thicker and thus stiffer shell causing these correction factors to remain near unity for small load levels.

As stated previously, the present work is the first attempt to evaluate quantitatively the effect of plasticity occurring at the tips of a bulging crack. In the presence of plasticity, the stress intensity factors are no longer theoretically valid fracture parameters, and the T^*-integral may be used. For a monotonically loaded elastic-plastic structure, T^* has the meaning of an energy-flux to the crack tip. For an elastic-plastic structure with growing cracks, T^*_ϵ has the meaning of an energy flux to the process-zone of size 'ϵ' near the crack tip. It is valid for the behaviour occurring in all three hierarchical models (global: linear elastic; intermediate: geometrically nonlinear elastic; and local: both geometrically and materially nonlinear). The effect of both the geometric nonlinearity *and* the plasticity is quantified in Figs. 12 and 13 by the correction factor of Eq. (23). The effect of the plasticity alone upon T^* is quantified in Fig. 14 by plotting the ratio of T^*_1 to T^*_{1l}, where T^*_1 is computed both with and without plasticity. The plot in Fig. 14 demonstrates that the plasticity results in a reduction of T^*_1. (Geometric nonlinearity is present for both cases. The cases with no plasticity were computed using the energy release rate of the geometrically nonlinear solution using the technique described in Potyondy (1993). This approach was verified for Case 1 where the energy release rate computed using this method (1.090 kips/inch) was compared to the value of T^*_1 (1.010 kips/inch) computed by turning off the plasticity in the local model and using the EDI method. An additional verification was obtained by comparing the energy release rates for Cases 3 and 4 to energy release rates obtained by Rankin, Brogan, and Riks (1993). For Case 3, the energy release rate was 2.7% less than Rankin's value, and for case 4, it was 7.9% less.)

Additional qualitative information about the plasticity occurring at the crack tip is presented in Figs. 15 and 16 where the size and shape of the plastic zone at the shell midsurface

under the full applied loading is shown. The plastic strains at the eight Gauss points of the 20-noded brick elements were averaged through the thickness to obtain a value on the midsurface which was then depicted as a color contoured image such that a positive plastic strain indicates the presence of plasticity. For all eight example cases, the plastic zone shape is that expected for a plane stress crack, and the diameter is between 0.7 and 0.9 inches (approximately 14 and 12 percent of the half crack length). The effect of offsetting the crack toward the stringer causes the plastic zone to become skewed in the direction away from the nearest stringer (cf. Fig. 16). The longitudinal and hoop stresses on the shell midsurface (defined in terms of the deformed shell coordinates) are presented in Figs. 17 and 18 for the offset crack of Case 6. Offsetting the crack significantly effects the symmetry of the longitudinal stress but has little effect on the symmetry of the hoop stress. The longitudinal stress is skewed in the same way as the plastic zone (compare Figs. 16 and 17).

The phenomenon of flapping is an important issue in the design and structural evaluation of aircraft. A survey of various crack path stability criteria and their application to flapping is provided by Zaal (1992). None of the existing criteria account for plasticity directly. We do not develop an explicit criteria for flapping here; rather, the following discussion will suggest a possible mechanism for flapping and explore its application to the example cases.

Flapping results from the large nonlinear deformation which causes an increase in the longitudinal stress parallel to the crack. It is postulated that for a crack of sufficient length, the longitudinal stress acting on a plane perpendicular to the crack and straight above the tip will reach a critical value causing the material on this plane to separate and thereby allowing the crack to flap. The variation of the longitudinal stress (normalised by the yield stress, σ_y = 47.0 ksi) acting on the line where this plane intersects the shell midsurface is presented in Figs. 19, 20, 21, and 22. These values were obtained by transforming the Gauss point stresses from the global coordinates to the deformed shell coordinates, then extrapolating and averaging these values at the row of nodes directly above and below the crack tip. As one would expect, the longer crack has higher values (cf. Fig. 19). Although the values of the stiffened cases are smaller than those of the unstiffened cases away from the crack, they grow faster as the crack tip is approached (cf. Figs. 20 and 21). Offsetting the crack causes the distribution of values to become unsymmetric, with greater values on the side away from the nearest stringer (cf. Fig. 22). An examination of the longitudinal stress contour in Fig. 17 indicates that the longitudinal stress does not attain a maximum directly above the crack tip but rather at some finite distance away from the crack tip.

5 Limitations of the Methodology and Discussion

One of the main drawbacks of the present methodology is that a crack which is very close to a stiffener cannot be modeled easily at the local level. Also the analysis of long cracks in lap joints (formed due to the coalescence of MSD) is not feasible with this methodology. A possible remedy is to cast the equations of hypoelastic-plasticity into shell space, and also develop a formulation of the Equivalent Domain Integral method for shell space analysis (cf. Appendix).

A few comments on the hierarchical strategy are in order. The hierarchical strategy involves a transfer of kinematic boundary conditions between models of differing idealisation (shell/solid). An added complication is that two of these models are nonlinear. An estimate of the errors accumulated in this process is not available. Also, the transfer of traction boundary conditions has not been investigated. A transfer of kinematic boundary conditions results in a stress mismatch along the boundary, while a transfer of traction boundary conditions results in a displacement mismatch. It is not clear how these mismatches affect the computed values of the T^*-integral. Theoretical and numerical study of the errors that develop in hierarchical modeling are required to determine the quality of a general hierarchical strategy.

It should be noted that the elastic constitutive equations of the intermediate model are different from those of the local model. The intermediate model is based on a hyperelastic equation

$$\begin{aligned} \mathbf{S} &= \frac{\partial W}{\partial \mathbf{E}} \\ W &= \frac{1}{2}\mathbf{E} : \mathbf{C} : \mathbf{E} \end{aligned} \tag{24}$$

where $\mathbf{S}$ is the second Piola-Kirchhoff stress tensor. The elastic behaviour in the local model is governed by a linear hypoelastic equation (Eq. (11)). It has been shown that these two formulations are not equivalent (Noll (1955); Bernstein (1960)). The consequence of this difference has not been investigated.

6 Concluding Remarks

A computational methodology for obtaining the nonlinear fracture parameters which account for the plasticity and large deformation occurring at the tip of a bulging crack in a pressurised fuselage has been presented. The methodology employs a hierarchical modeling of the fuselage with three stages. The first stage (global) is a linear shell analysis, the second stage (intermediate) is a geometrically nonlinear shell analysis, and the final stage (local) is a 3D finite deformation elastoplastic analysis of the cracked skin. The T^*-integral, which accounts for the large deformation and plasticity, is evaluated from the equilibrium state of the local model using the Equivalent Domain Integral method which has proven to be a powerful technique for evaluating energy-flux based integral fracture parameters. The effectiveness of the methodology was demonstrated through several example problems. Correction factors, which account for the effect of plasticity and large deformation, relating the nonlinear T^* values to those obtained from a linear elastic stiffened shell analysis, were computed. The issue of flapping was addressed by investigating the behaviour of the longitudinal stress parallel to the crack.

Acknowledgments

This research is supported under a grant to the Center of Excellence for Computational Modeling of Aircraft Structures at Georgia Institute of Technology, from the Federal Aviation Administration. The authors also thank Dr. R. Singh, Mr. V. Nagaswamy, Mr. L. Wang for many helpful discussions. The first author also wishes to express his heartfelt thanks to S. for helping him through some turbulent times of his life.

Appendix : The EDI Method for Shell Space Analysis

The Equivalent Domain Integral (Nikishkov and Atluri (1987)) method is a convenient and accurate method for the evaluation of the energy-flux based integral fracture parameters. The method presented in Nikishkov and Atluri (1987) is for arbitrary three-dimensional cracks. We describe here a generalisation of this method for finite deformation such that the fracture parameters may be evaluated from the equilibrium state obtained from a (possibly geometrically nonlinear) shell space finite element analysis.

Using the equations of equilibrium (Eq. (4)), under the absence of body forces, the volume integral in (Eq. (22)) may be split as

$$
\begin{aligned}
T^*_{\epsilon\alpha}\Delta &= -\int_{V-V_\epsilon}\left[\frac{\partial}{\partial X_\alpha}(W) - \left(T_{ij}\frac{\partial^2 u_j}{\partial X_i \partial X_\alpha}\right)\right] s dV \\
&\quad -\int_{V-V_\epsilon}\left[\frac{\partial s}{\partial X_\alpha}W - \frac{\partial s}{\partial X_i}\left(T_{ij}\frac{\partial u_j}{\partial X_\alpha}\right)\right] dV
\end{aligned}
\tag{25}
$$

The evaluation of the two integrals in Eq. (25) is described in Nikishkov and Atluri (1987). It requires knowledge of the stresses and strain energy density (work density, in the case of elasto-plastic materials) at the Gauss integration points of the elements (2×2, for bricks).

For the evaluation of the T^*-integral using the solution obtained in a shell analysis, we propose the following method. We present the description for four noded quadrilateral (Q4) shell elements with 2×2 integration. First, construct a brick element (8-noded, B8) such that the Q4 forms the midsurface (cf. Fig. 23) using the normals at the nodes of the Q4. It is clear that the Gauss points of the B8 projected onto the midsurface will be the Gauss points of the Q4 (for example, the projection of the point **A** is the point **B**, cf. Fig. 23). The displacements at the nodes of the B8 element are obtained using the Kirchhoff-Love assumptions

$$
\begin{aligned}
u_\alpha &= u^o_\alpha + z\phi_\alpha \\
u_3 &= w(x,y)
\end{aligned}
\tag{26}
$$

where u^o_α is the in-plane displacement of the mid-surface, ϕ_α are the rotations, w is the out-of-plane displacement, and z is the thickness coordinate. The second Piola-Kirchhoff stress may be obtained at the gauss points using

$$
\begin{aligned}
S_{\alpha\beta} &= \frac{1}{h}\left[N_{\alpha\beta} + \frac{12z}{h^2}M_{\alpha\beta}\right] \\
S_{\alpha 3} &= \frac{3}{2h}\left[1 - \left(\frac{2z}{h}\right)^2\right] Q_\alpha
\end{aligned}
\tag{27}
$$

where $N_{\alpha\beta}$ are the stress resultants, $M_{\alpha\beta}$ are the moment resultants, and Q_α are the shear resultants at the Gauss points of the Q4 element. The gradient of deformation tensor **F**,

may be evaluated at the Gauss point of the B8 from the nodal displacements and the B8 shape functions. The first Piola-Kirchhoff tensor may now be evaluated using

$$\mathbf{T} = \mathbf{S}\mathbf{F}^T. \tag{28}$$

The elastic strain energy density at the Gauss points may be evaluated using the elastic constitutive equations as

$$W = \frac{1}{2} S_{ij} E_{ij} \tag{29}$$

where E_{ij} are the Green-Lagrange strains (these are easily obtained if $\mathbf{F}$ is available (Eq. (3))). For the elasto-plastic case, the Gauss point may be chosen as an integration station, and the work density may be stored. Thus, all the quantities for the computation of the two integrals in Eq. (25) are available at the Gauss points of the B8, and integration may be carried out as described in Nikishkov and Atluri (1987). We suggest the use of an s-function which is constant through the thickness (type(d) function of Nikishkov and Atluri (1987)) for the B8 element. (It has been shown (Nikishkov and Atluri (1987)) that the computed values of the integral are not sensitive to the choice of the s-function.)

References

Almroth, B.O.; Brogan, F.A.; Stanley, G.M. (1986): Structural analysis of general shells, users instructions for STAGSC-1, Vol. 2, Lockheed Missiles and Space Company, LMSC D633873.

Ansell, H. (1988): Bulging of cracked pressurised aircraft structures, LIU-TEK-LIC-1988:11, Institute of Technology, Dept. of Mech. Engg., S-581-83, Lingkoping, Sweden.

Ashwell, D. G.; Sabir, A. B. (1972): A new cylindrical shell finite element based on simple independent strain functions. Int. J. Mech. Sci., 14, 171-183.

Atluri, S. N. (1980): On some new general and complementary energy theorems for the rate problems in finite strain, classical elastoplasticity. J. Struct. Mech., 8, 61-92.

Atluri, S. N. (1982): Path-independent integrals in finite elasticity and inelasticity, with body forces, inertia, and arbitrary crack-face conditions. Engg. Frac. Mech., 16, 341-364.

Atluri, S. N. (1984): Alternate stress and conjugate strain measures, and mixed variational formulations involving rigid rotations, for computational analyses of finitely deformed solids, with application to plates and shells - I. Computers and Structures, 18, No. 1, 93-116.

Atluri, S. N. (1986): Energetic approaches and path-independent integrals in fracture mechanics. In: Computational Methods in the Mechanics of Fracture, Atluri, S.N. ed., Elsevier Science Publishers B.V.

Atluri, S. N.; Tong, P. (1991): Computational schemes for integrity analyses of fuselage panels in aging airplanes. In: Structural Integrity of Aging Airplanes, Springer Series in Computational Mechanics, Atluri. S.N.; Sampath, S.G.; Tong, P. eds, Springer-Verlag, Berlin.

Bernstein, B. (1960): Hypoelasticity and elasticity. Arch. Rat. Mech. Anal., 6, No. 2, 89-104.

Chen, D. (1990): Bulging of fatigue cracks in a pressurised aircraft fuselage. Faculty of Aerospace Engineering, Delft University, Delft, The Netherlands, Report LR-647.

Chen, D.; Schijve, J. (1991): Bulging of fatigue cracks in a pressurised aircraft fuselage. Faculty of Aerospace Engineering, Delft University, Delft, The Netherlands, Report LR-655.

Gray, L. J.; Potyondy, D.O.; Lutz, E. D.; Wawrzynek, P.A.; Martha, L.F.; Ingraffea, A.R. (1994): Crack propagation modeling. To appear in Mathematical Models and Methods in Applied Sciences.

Hill, R. (1968): Some basic principles in the mechanics of solids without a natural time. J. Mech. Phys. Solids, 7, 209-225.

Hui, C.Y.; Zehnder, A.T. (1993): A theory for the fracture of thin plates subjected to bending and twisting moments. Int. J. Fracture, 61, 211-229.

Hutchinson, J.W. (1968): Singular behaviour at the end of a tensile crack in hardening material. J. Mech. Phys. Solids, 16, 13-31.

Koiter, W.T. (1966): On the nonlinear theory of thin elastic shells. Proc. Kon. Ned. Ak. v. Wetensch., 1-54.

Lemaitre, J.; Turbat, A.; Loubet, R. (1977): Fracture mechanics analysis of pressurised cracked shallow shells. Engg. Frac. Mech., 9, 443-460.

Miller, M.; Kaelber, K.N.; Worden, R.E. (1992): Finite element analysis of pressure vessel panels. In: Durability of metal aircraft structures, Proceedings of the International Workshop on Structural Integrity of Aging Airplanes, March 31-April 2, 1992, Atlanta, Atluri, S.N.; Harris, C.E.; Hoggard, A.; Miller, N.; Sampath, S.G. eds., 337-348.

MIL-HDBK-5E (1987): Metallic materials and elements for aerospace vehicle structures. Military standardization handbook, U. S. Dept. of Defense.

Nikishkov, G. P.; Atluri, S. N. (1987): Calculation of fracture mechanics parameters for arbitrary three-dimensional crack by the equivalent domain integral method. Int. J. Num. Meth. Engg., 24, 1801-1821.

Nikishkov, G. P.; Atluri, S. N. (1994): Implementation of a generalised midpoint algorithm for integration of elastoplastic constitutive relations for Mises hardening material. To appear in Computers and Structures.

Noll, W. (1955): On the continuity of the solid and fluid states. J. Rat. Mech. Anal., 4, No. 1, 3-81.

Nour-Omid, B.; Rankin, C.C. (1991): Finite rotation analysis and consistent linearisation using projectors. Comp. Meth. Appl. Mech. Engg., 93, 353-384.

Potyondy, D.O. (1993): A software framework for simulating curvilinear crack growth in pressurised thin shells. Ph.D. Thesis, Cornell University, Ithaca, NY.

Rankin, C.C; Brogan, F.A. (1991): The computational mechanics testbed structural element processor ES5: STAGS shell element. NASA contractor report 4358.

Rankin, C. C.; Brogan, F. A.; Riks, E. (1993): Some computational tools for the analysis of through cracks in stiffened fuselage shells. J. Comp. Mech., 13, 143-156.

Rice, J.R.; Rosengren, G.F. (1968): Plane strain deformation near a crack tip in a power-law hardening material. J. Mech. Phys. Solids, 16, 1-12

Riks, E. (1984): Some computational aspects of the stability analysis of nonlinear structures. Comp. Meth. Appl. Mech. Engg., 47, 219-249.

Riks, E. (1987): Bulging cracks in pressurised fuselages: a numerical study. NLR-MP-87058 U, The Netherlands.

Riks, E. (1987a): Progress in collapse analysis. Journal of Pressure Vessel Technology, 109, 27-41.

Rubenstein, R.; Atluri, S. N. (1983): Objectivity of incremental constitutive relations over finite time steps in computational finite deformation analyses. Comp. Meth. App. Mech. Engg., 36, 277-290.

Singh, R.; Park, J. H.; Atluri, S. N.(1994): Growth of multiple cracks and their link-up in a fuselage lap joint. Communicated to J. AIAA.

Swift, T. (1987): Damage tolerance in pressurised fuselages. 11^{th} Plantema Memorial Lecture, McDonnell Douglas, Douglas Paper 7768.

Truesdell, C. (1955): Hypoelasticity. J. Rat. Mech. Anal., 4, No. 1, 83-133, 1019-1020.

Truesdell, C.; Noll, W. (1965): The nonlinear field theories of mechanics. Encyclopedia of Physics (Flugge, S. ed.), Vol. III/3, Springer-Verlag, Berlin.

Wang, L; Atluri, S.N. (1994): An analysis of an explicit algorithm and the radial return algorithm, and a proposed modification, in finite plasticity. To appear in Comp. Mech.

Zaal, K.J.J.M. (1992): A survey of crack path stability criteria and their application to crack flapping phenomena in stiffened structures. Faculty of Aerospace Engineering, Delft University, Delft, The Netherlands, Report LR-681.

Table 1: Load and geometric properties of the fuselage model.

Internal Pressure	8.0 psi
Radius	74.0 inches
Longitudinal Stiffener (Stringer)	Height - 1.0 inches
	Thickness - 0.342 inches
Circumferential Stiffener (Frame)	Height - 2.0 inches
	Thickness - 0.171 inches
Stringer Spacing	9.3 inches
Frame Spacing	20.0 inches

Table 2: Example problems.

Name	Stiffened	Crack Length (inches)	Offset (inches)	Skin Thickness (inches)
Case 1	No	10.0	-	0.036
Case 2	No	15.0	-	0.036
Case 3	Yes	10.0	0.0	0.036
Case 4	Yes	15.0	0.0	0.036
Case 5	Yes	10.0	2.08	0.036
Case 6	Yes	15.0	2.08	0.036
Case 7	Yes	10.0	0.0	0.072
Case 8	Yes	10.0	2.08	0.072

Table 3: Piecewise linear approximation of the Al2024-T3 flow curve.

Stress (ksi)	Plastic Strain
47.0	0.0
50.0	0.001538
53.0	0.006952
60.0	0.034286
65.8	0.073733

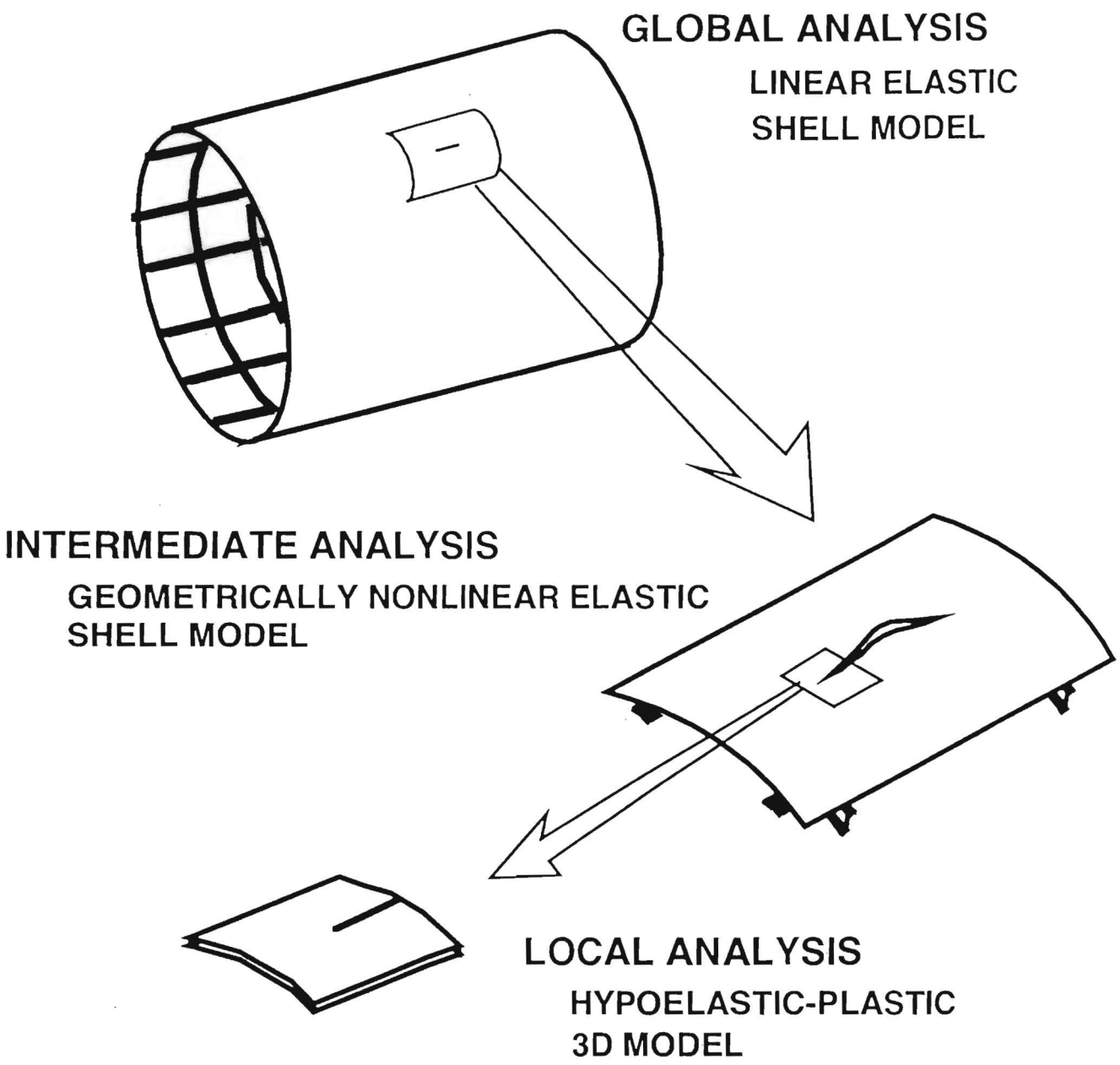

Figure 1: Hierarchical modeling strategy.

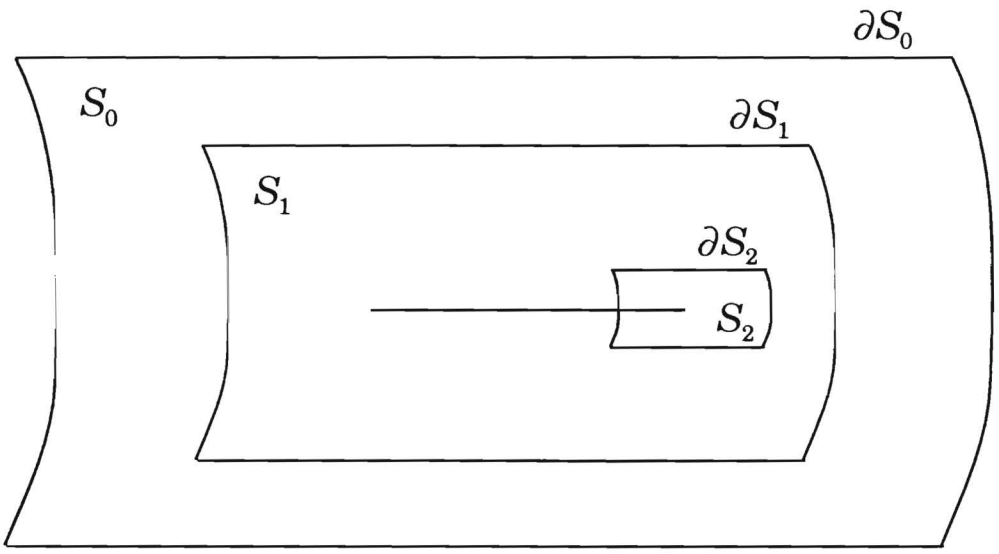

Figure 2: The shell surfaces S_i, and the boundaries ∂S_i, of the three hierarchical models (not drawn to scale).

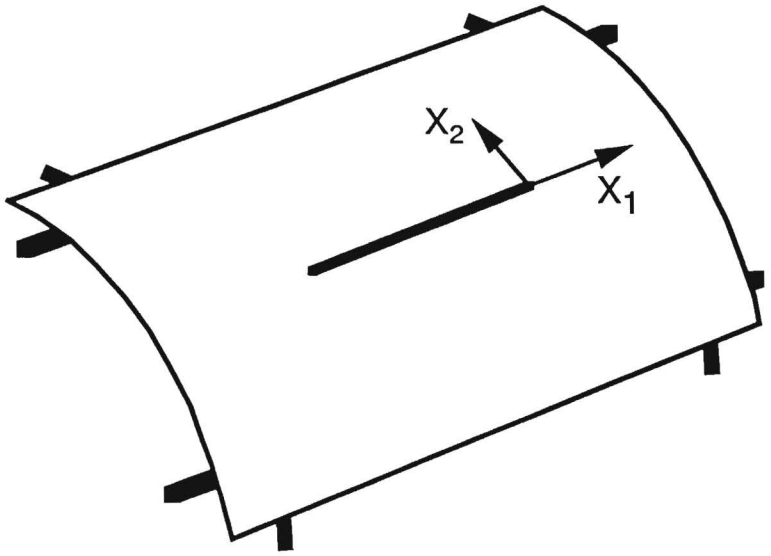

Figure 3: Crack tip coordinate system.

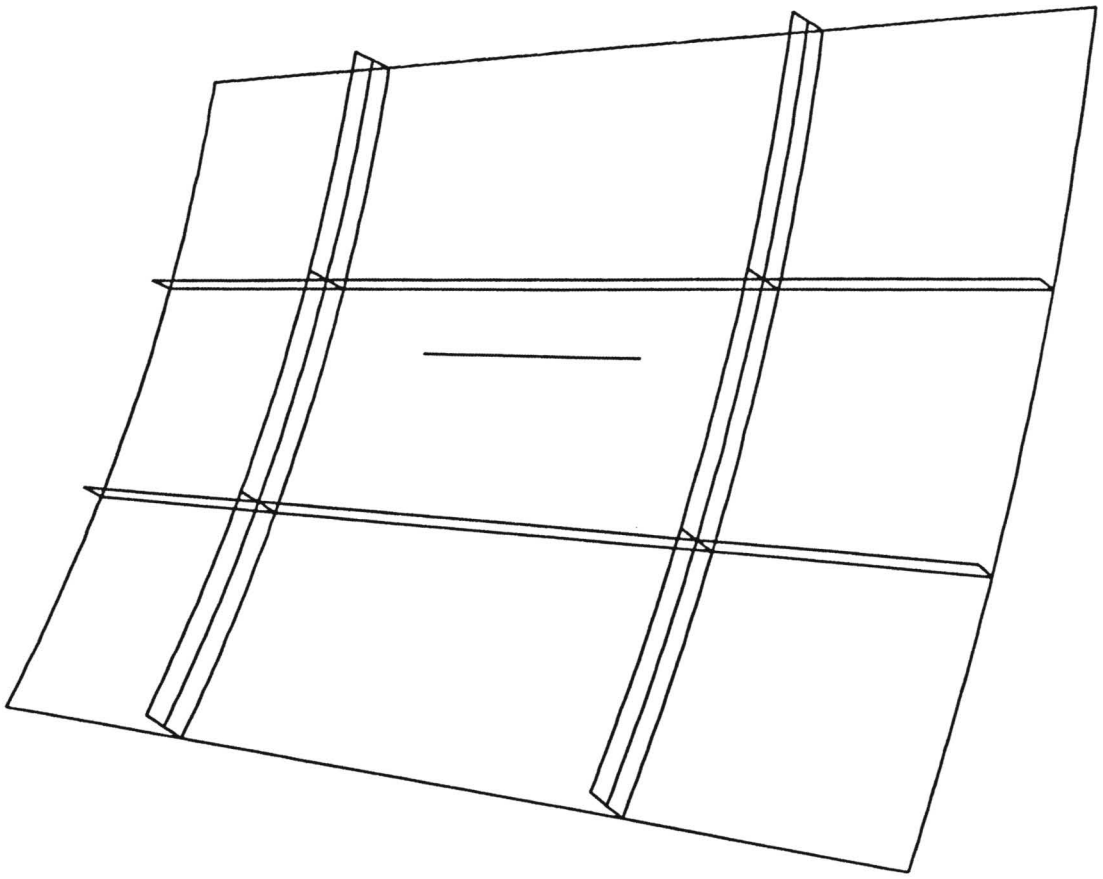

Figure 4: Example fuselage model.

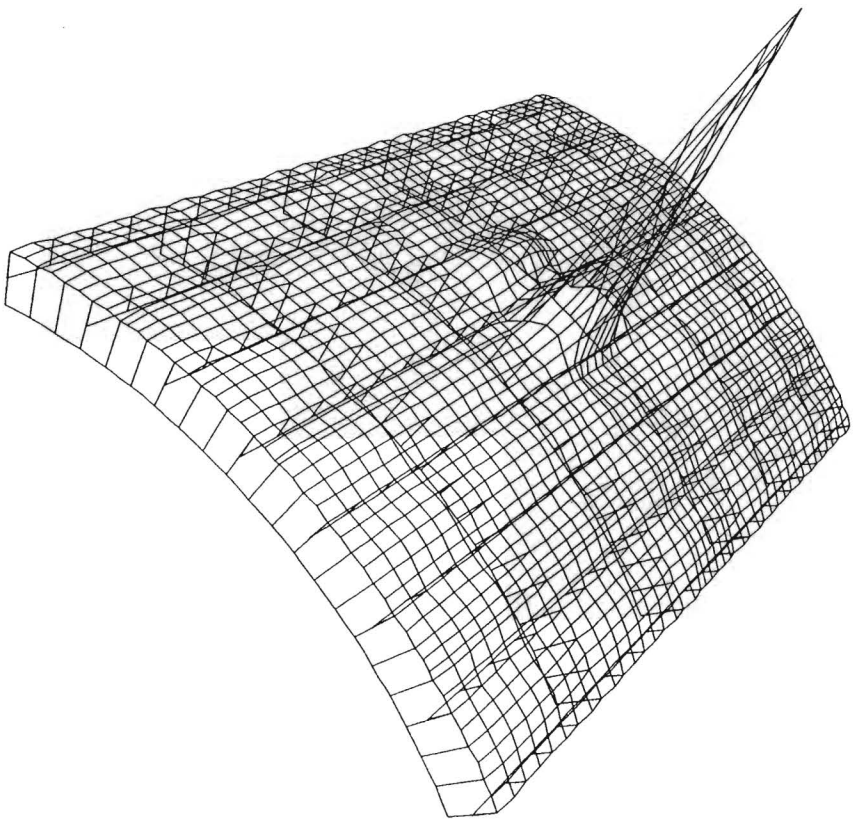

Figure 5: Deformed global model, Case 6 (magnification 5.0).

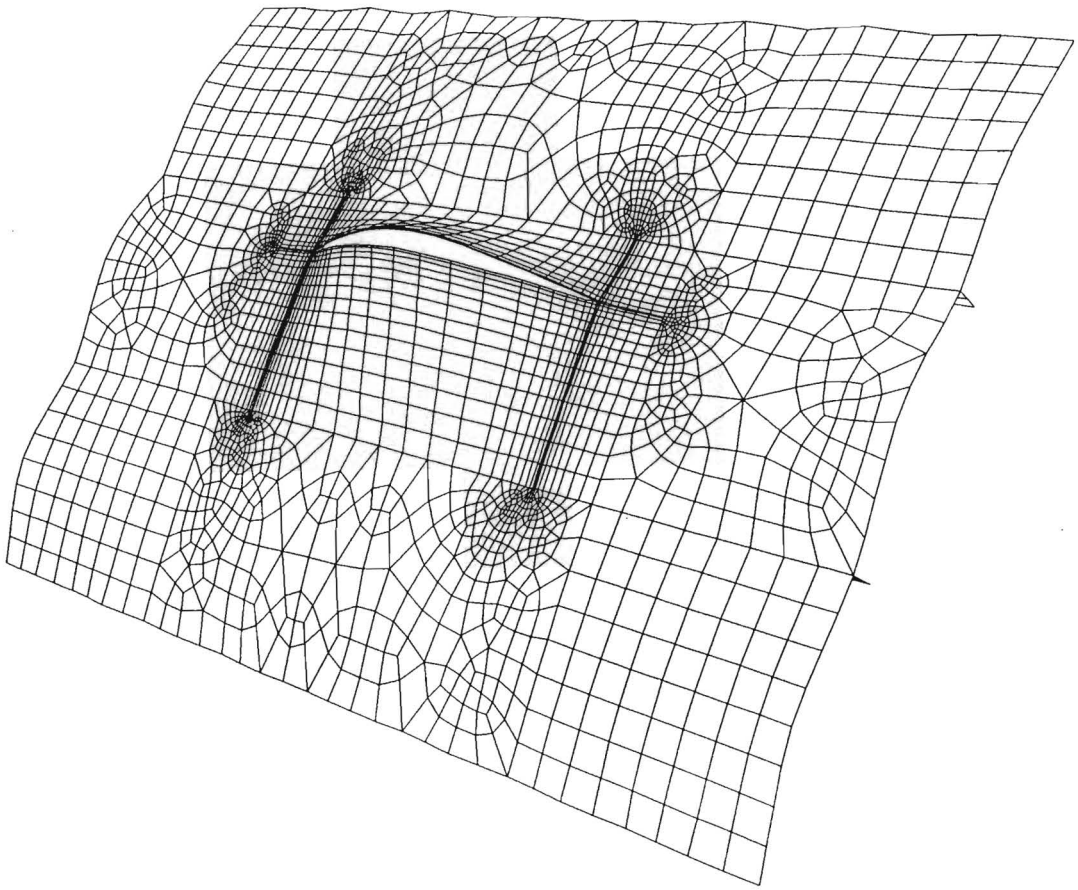

Figure 6: Deformed intermediate model, Case 6 (magnification 5.0).

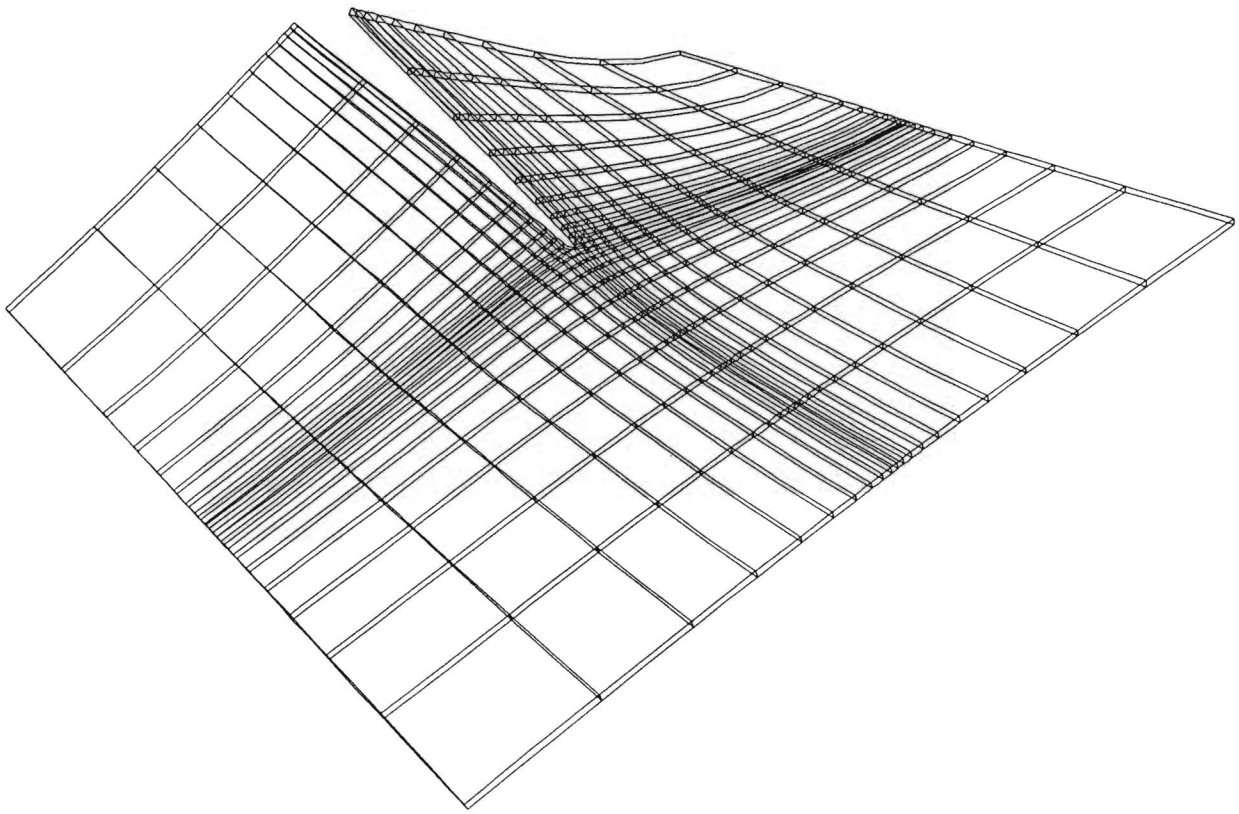

Figure 7: Deformed local model, Case 6 (magnification 5.0).

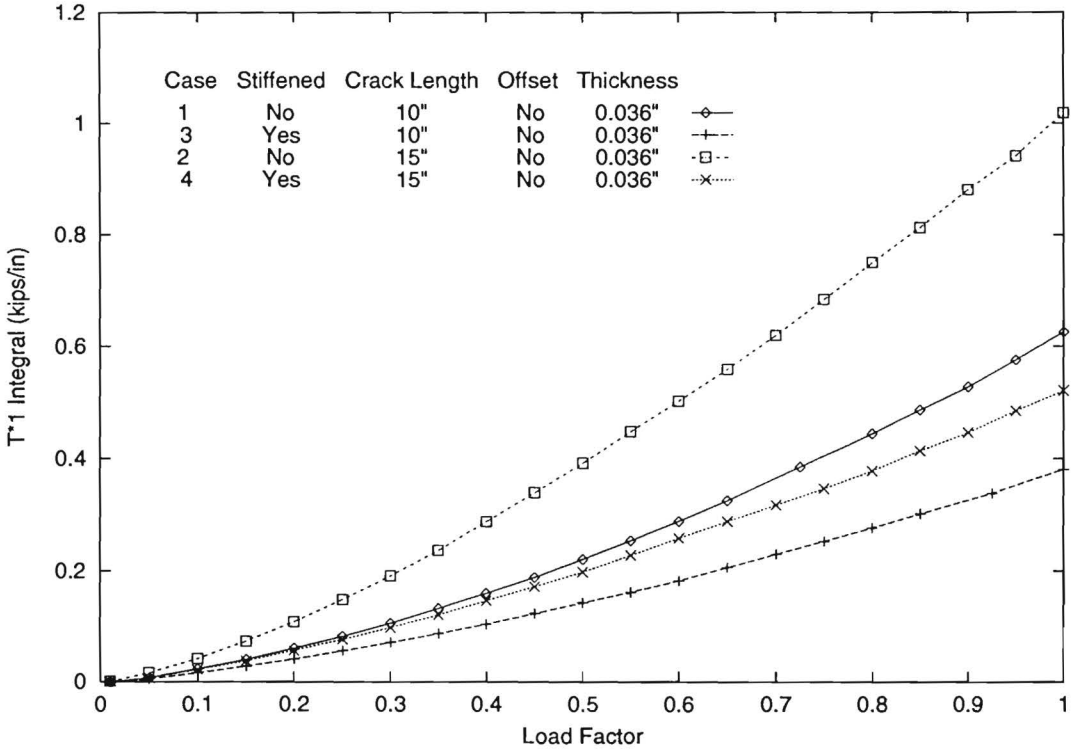

Figure 8: T_1^*-Integral, effect of stiffeners.

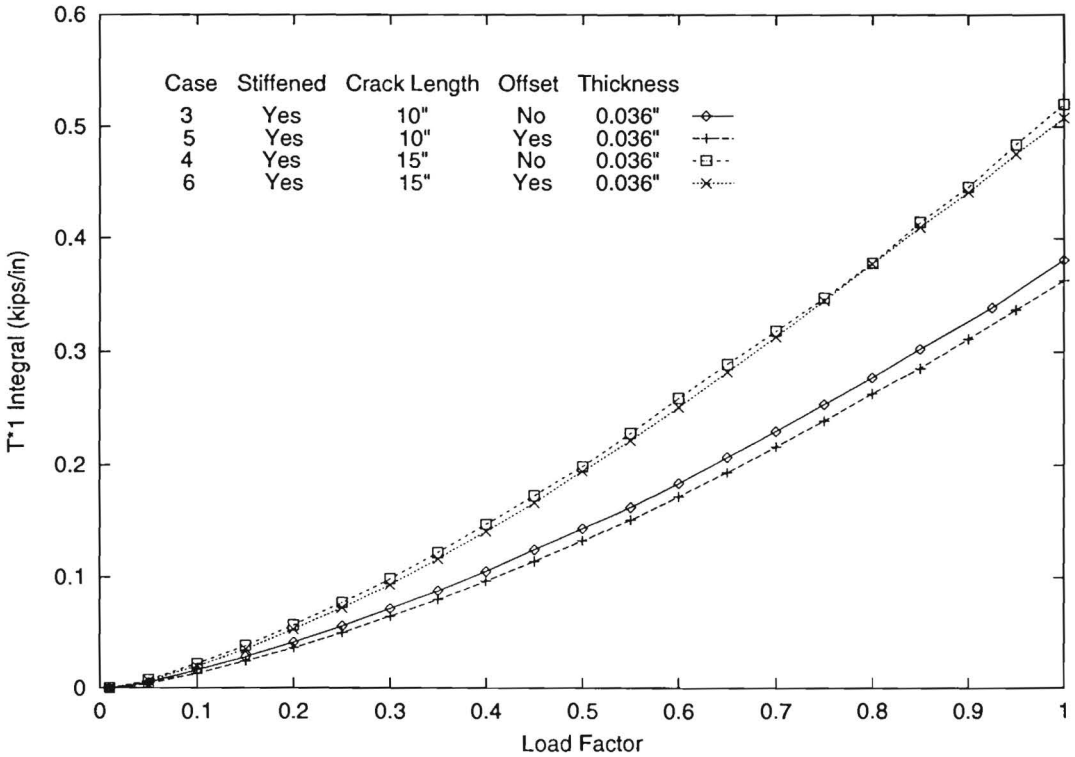

Figure 9: T_1^*-Integral, effect of offset.

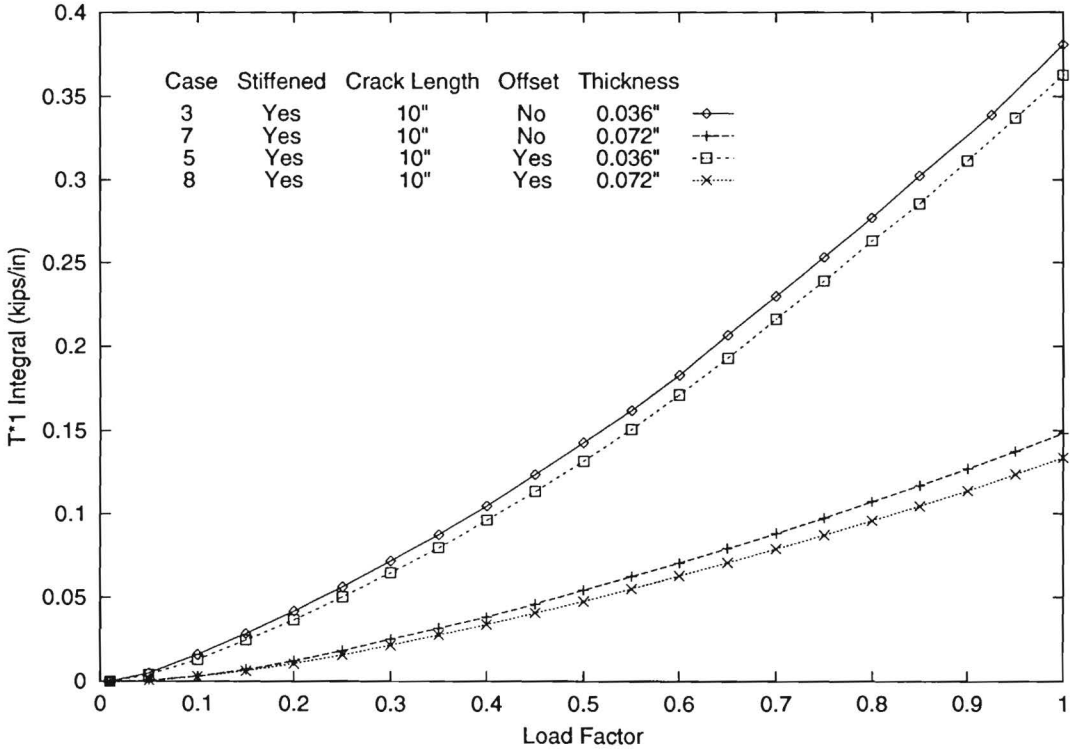

Figure 10: T_1^*-Integral, effect of skin gauge.

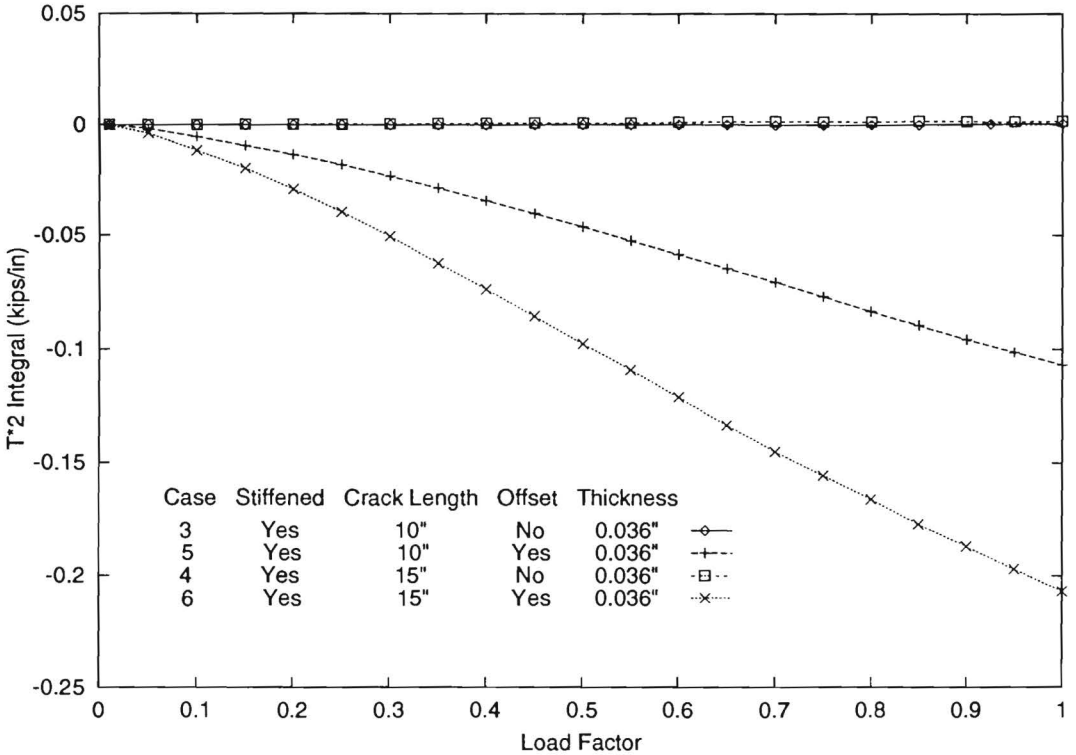

Figure 11: T_2^*-Integral

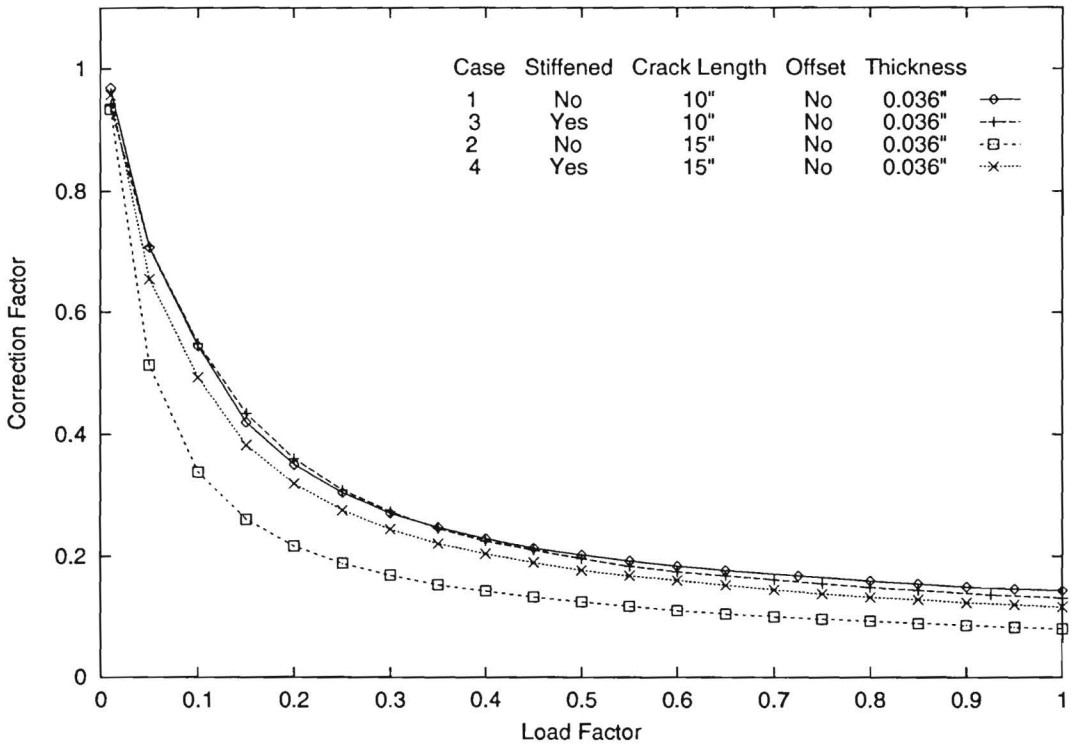

Figure 12: Correction factors, Cases 1-4.

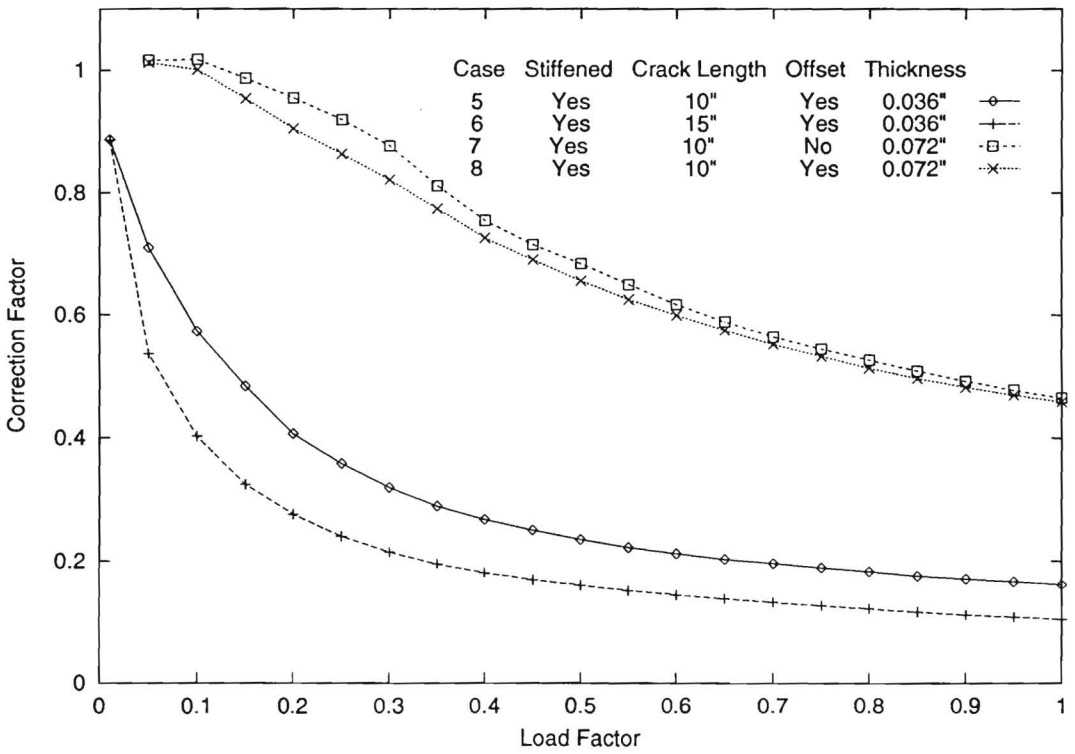

Figure 13: Correction factors, Cases 5-8.

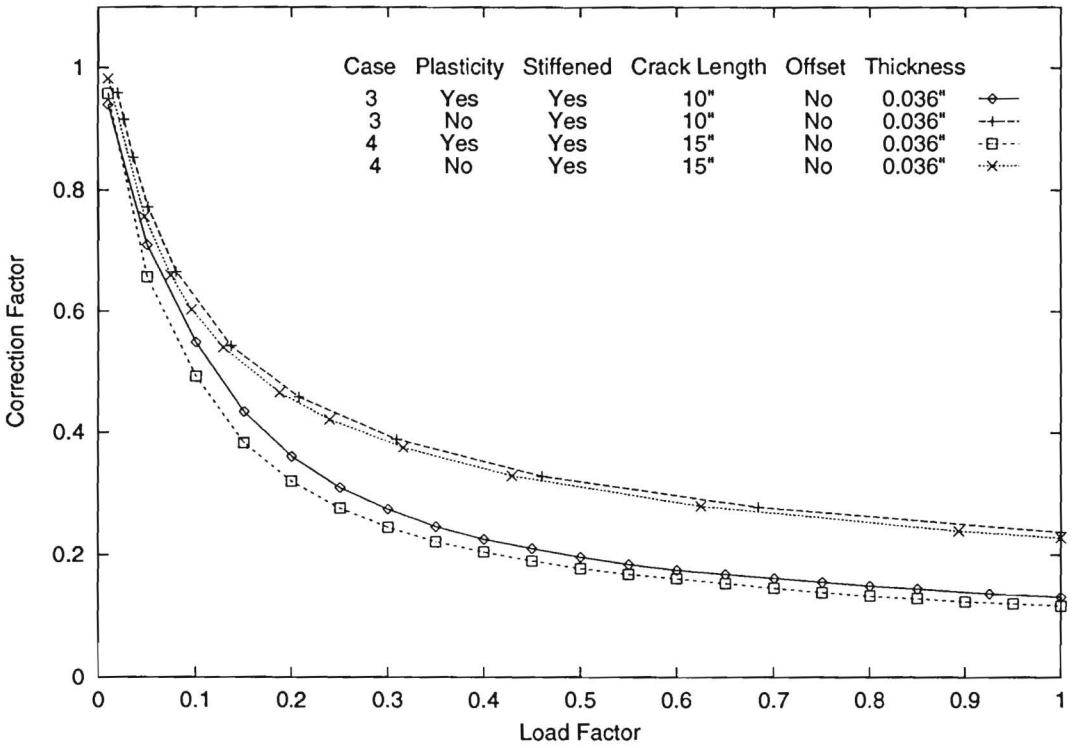

Figure 14: Correction factors both with and without plasticity.

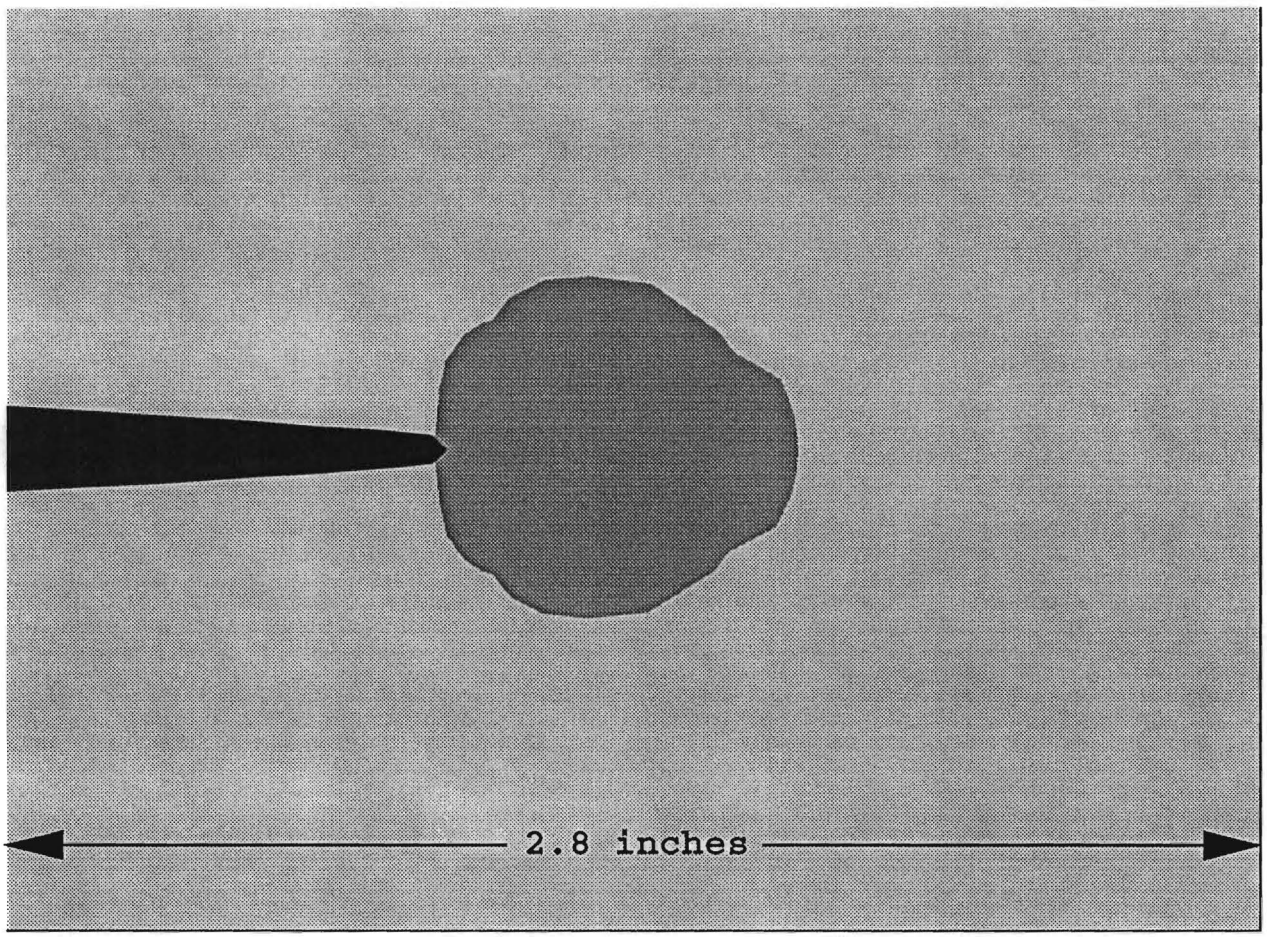

Figure 15: Plastic zone, Case 4 (drawn on deformed shape with magnification 5.0).

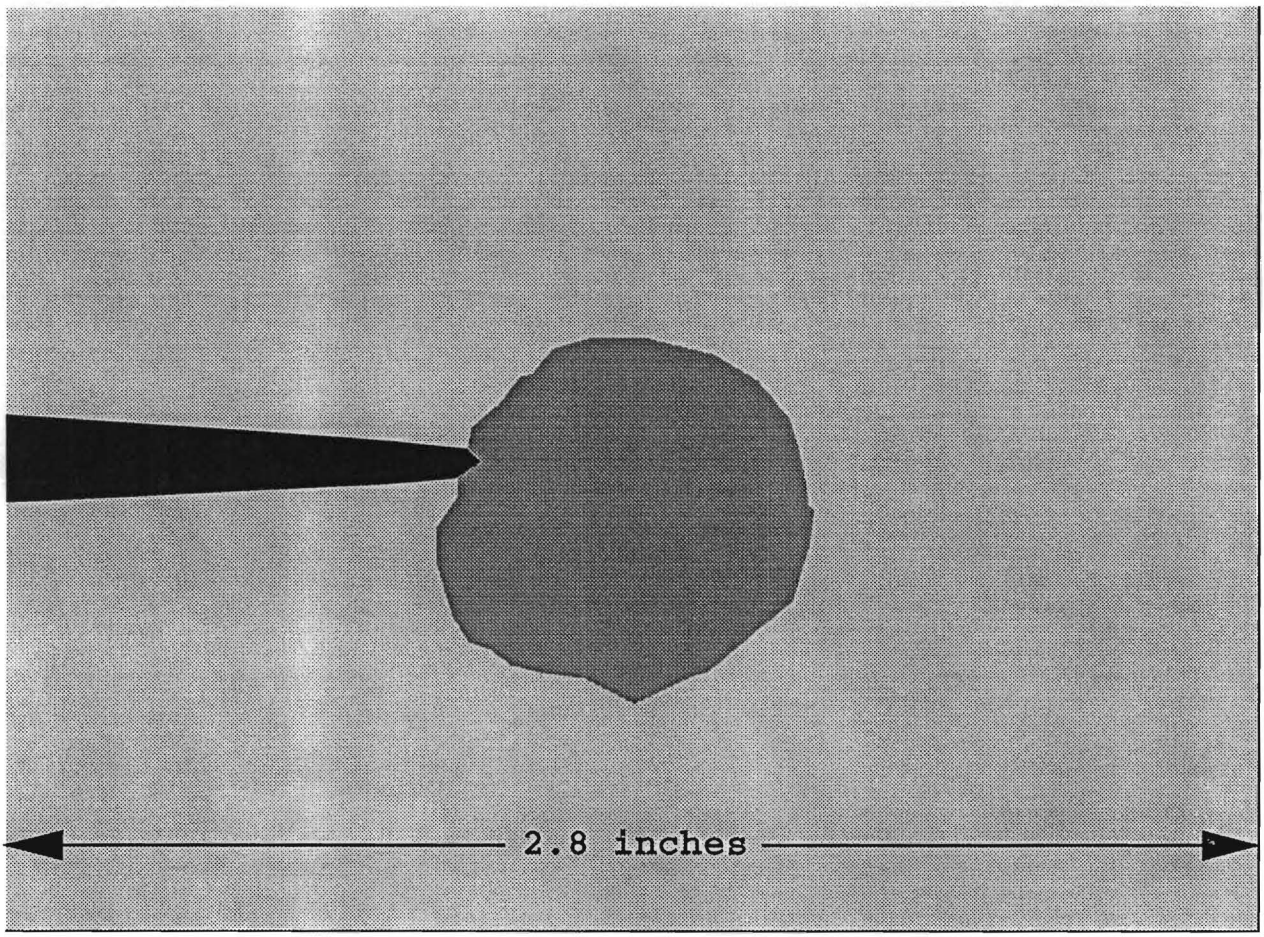

Figure 16: Plastic zone, Case 6 (drawn on deformed shape with magnification 5.0).

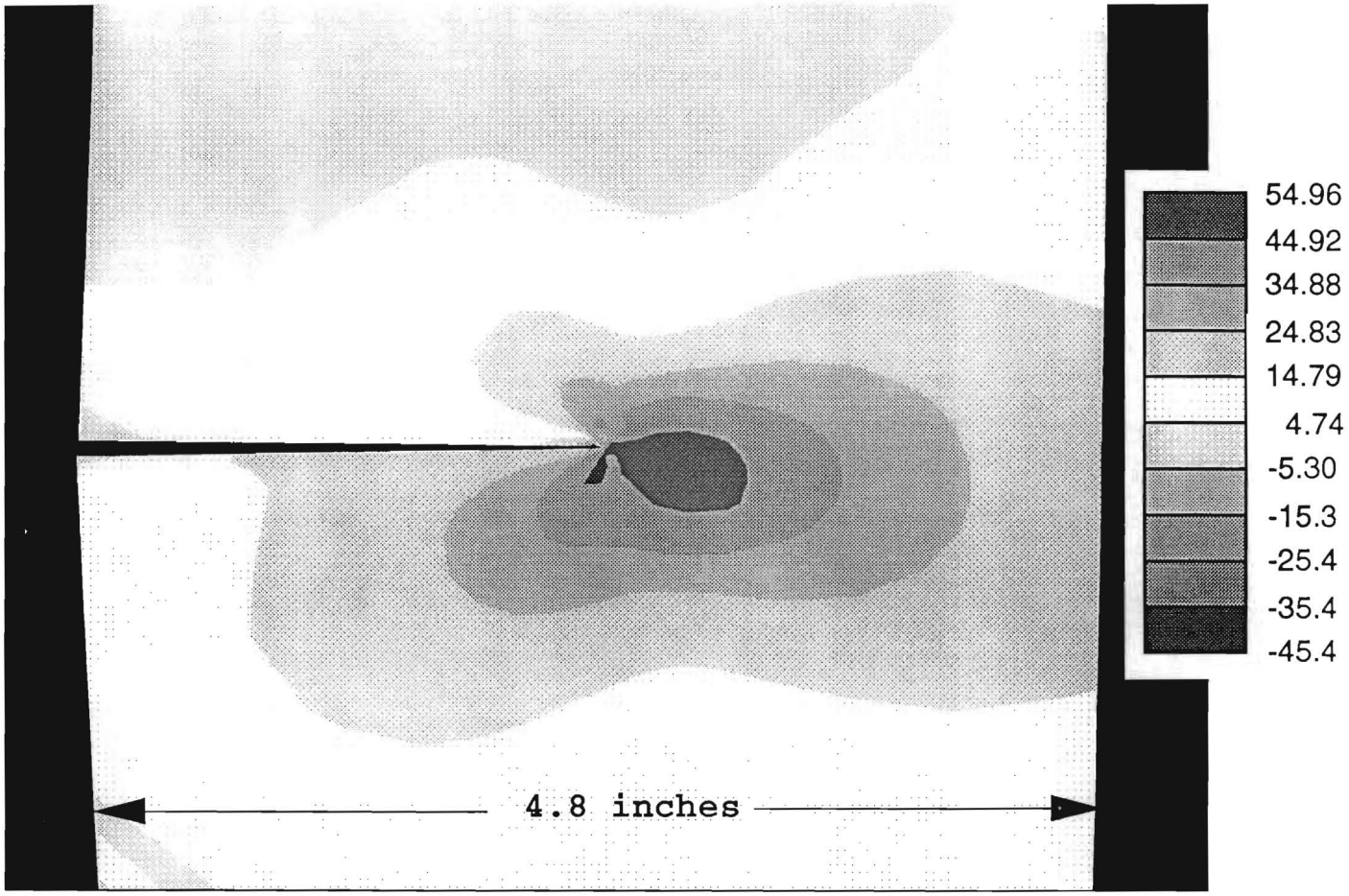

Figure 17: Longitudinal stress contour, values in ksi, Case 6 (drawn on deformed shape with magnification 1.0).

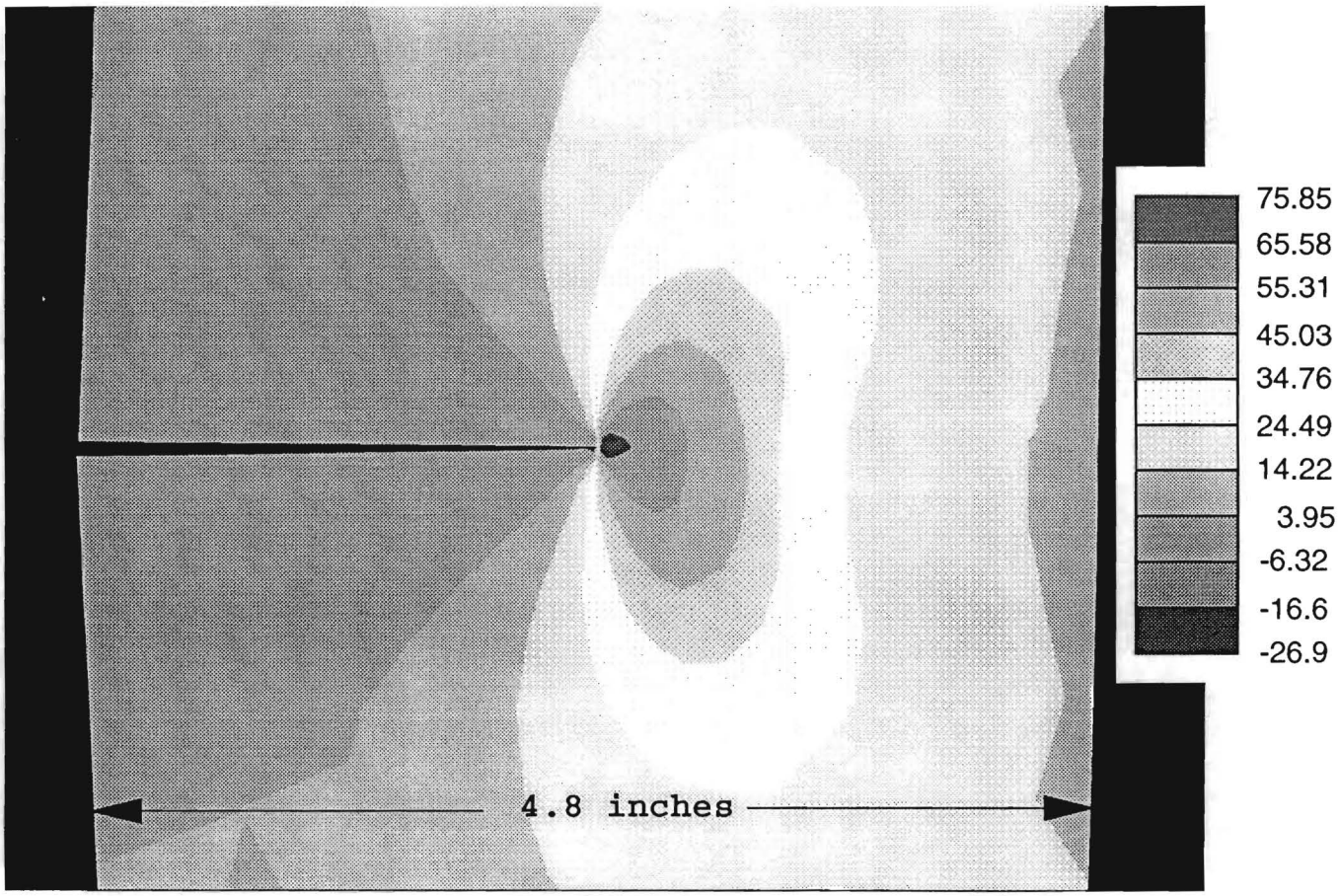

Figure 18: Hoop stress contour, values in ksi, Case 6 (drawn on deformed shape with magnification 1.0).

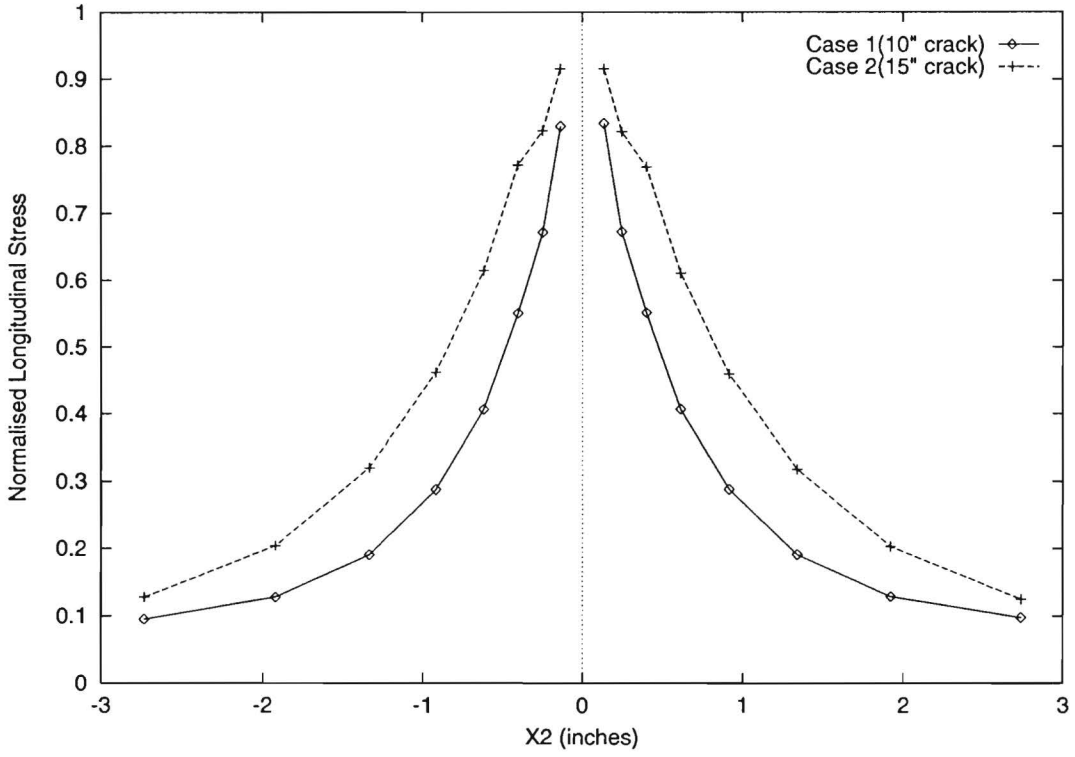

Figure 19: Normalised longitudinal stress (unstiffened cases).

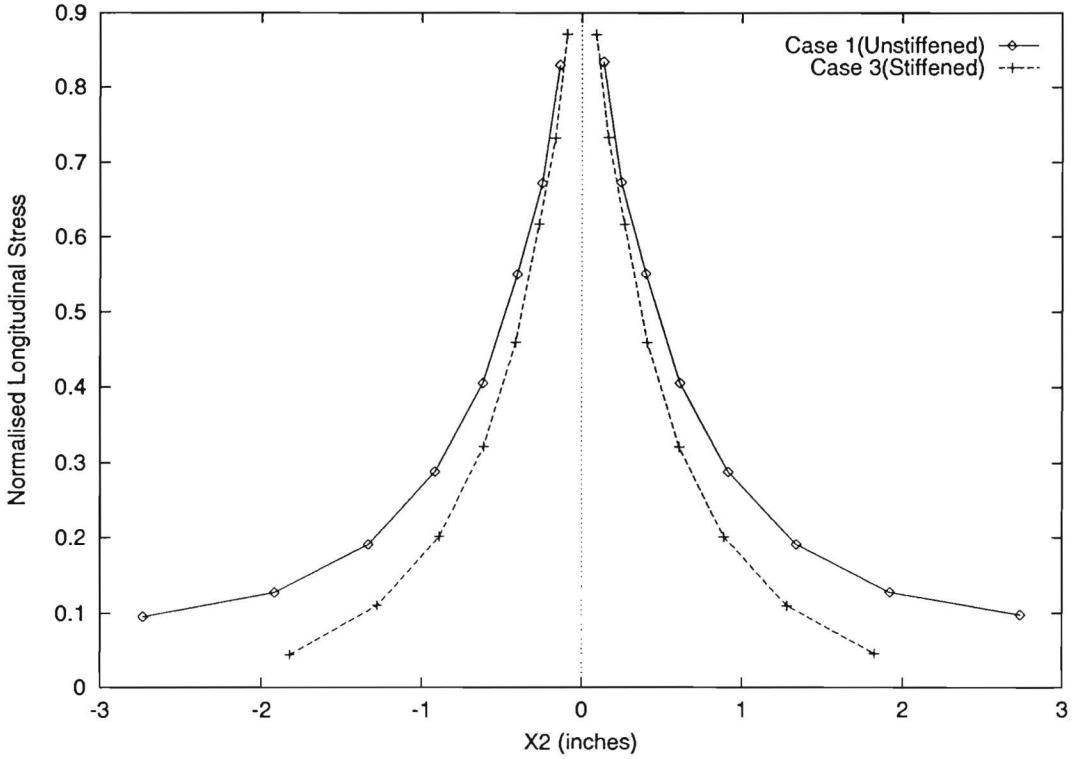

Figure 20: Normalised longitudinal stress (10 inch crack).

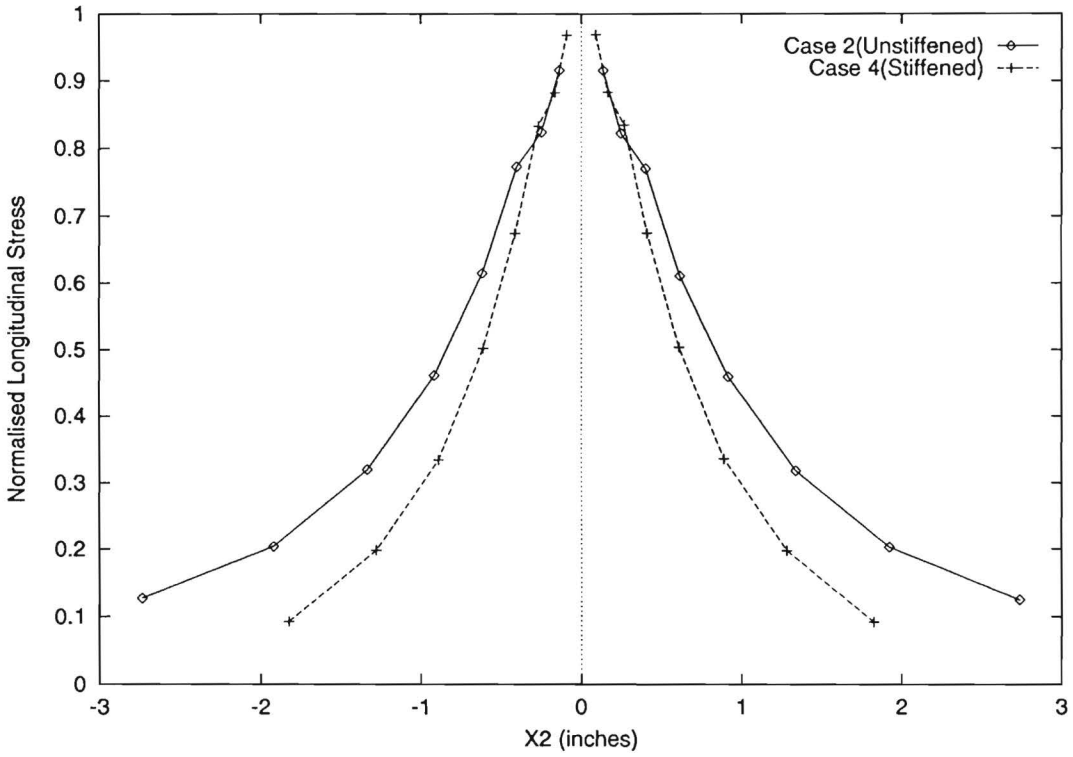

Figure 21: Normalised longitudinal stress (15 inch crack).

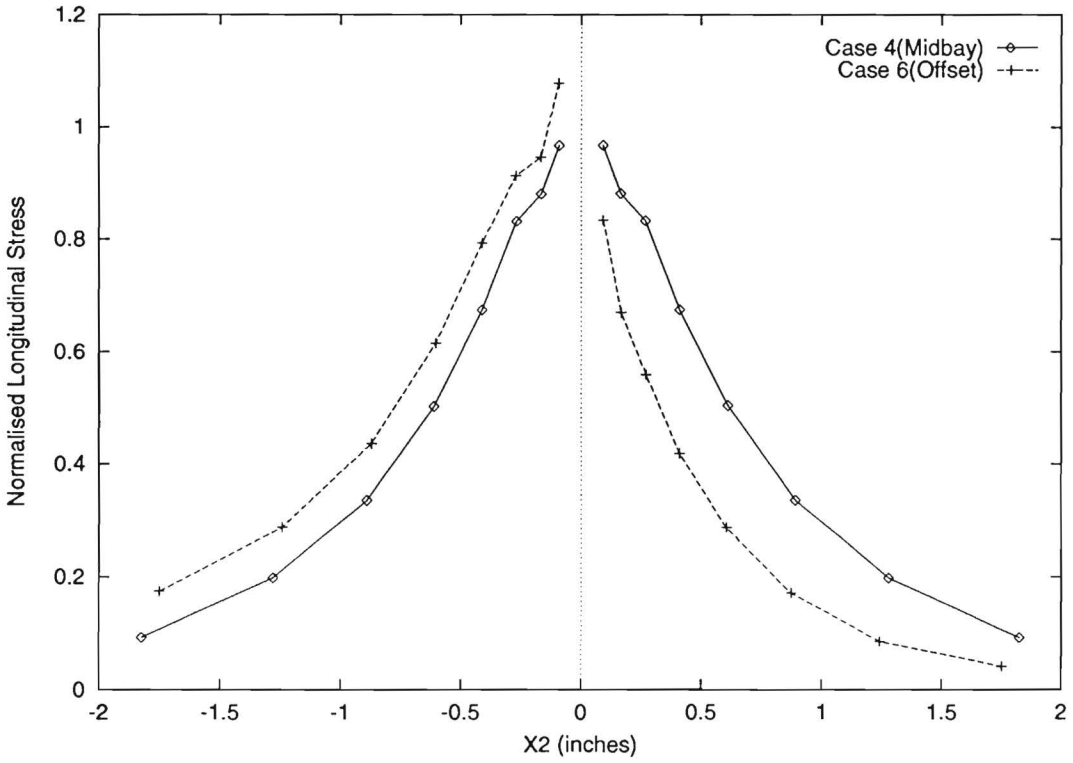

Figure 22: Normalised longitudinal stress (midbay vs offset).

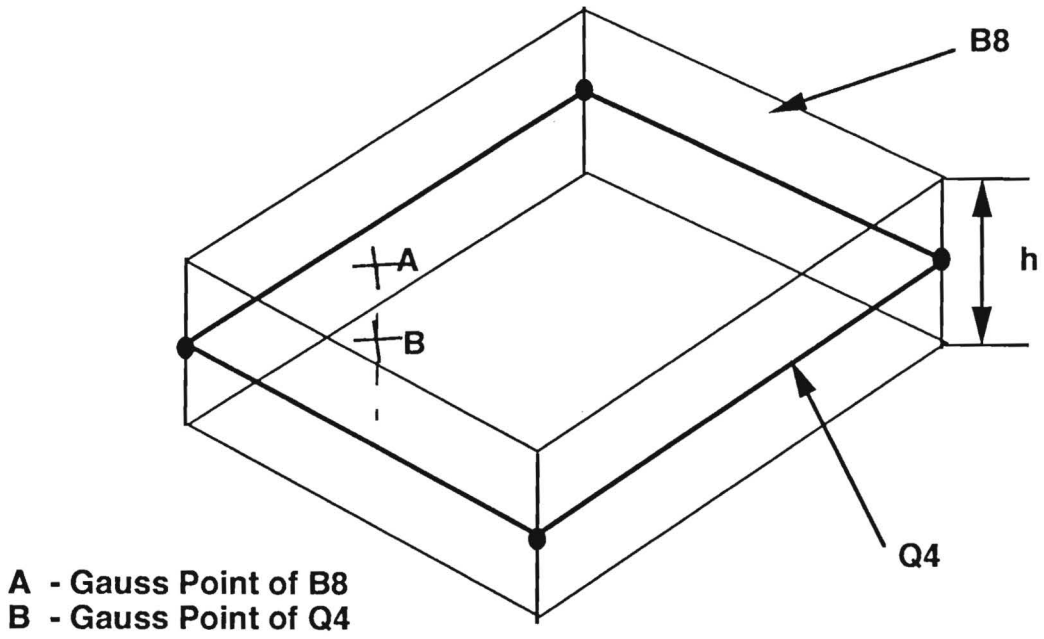

Figure 23: EDI method for shell space.